ERDC/GSL TR-14-38

Geotechnical and Structures Laboratory

US Army Corps
of Engineers®
Engineer Research and
Development Center

ERDC
INNOVATIVE SOLUTIONS
for a safer, better world

Airfield Damage Repair Modernization Program

AM2 3-4 Alternate Lay Pattern Evaluation

Timothy W. Rushing, Lyan Garcia, Jeb S. Tingle,
Paul G. Allison, and Craig A. Rutland

September 2014

The US Army Engineer Research and Development Center (ERDC) solves the nation's toughest engineering and environmental challenges. ERDC develops innovative solutions in civil and military engineering, geospatial sciences, water resources, and environmental sciences for the Army, the Department of Defense, civilian agencies, and our nation's public good. Find out more at www.erdc.usace.army.mil.

To search for other technical reports published by ERDC, visit the ERDC online library at http://acwc.sdp.sirsi.net/client/default.

ERDC/GSL TR-14-38
September 2014

AM2 3-4 Alternate Lay Pattern Evaluation

Timothy W. Rushing, Lyan Garcia, Jeb S. Tingle, and Paul G. Allison

Geotechnical and Structures Laboratory
U.S. Army Engineer Research and Development Center
3909 Halls Ferry Road
Vicksburg, MS 39180-6199

Craig A. Rutland

Engineering Division
Civil Engineering Branch
Air Force Civil Engineering Center
139 Barnes Drive, Suite 1
Tyndall AFB, FL 32403

Final report

Prepared for Headquarters, Air Force Civil Engineer Center
Tyndall Air Force Base, FL 32403-5319

Abstract

AM2 airfield matting has a long history of successful performance as an expeditionary airfield surfacing system. Logistical considerations for shipment of AM2 by the U.S. Marine Corps require equal numbers of 6-ft and 12-ft-long AM2 panels to be delivered to all project sites, resulting in far more 6-ft panels than are necessary to create a standard brickwork pattern. Therefore, the 3-4 alternate lay pattern was designed to allow Marines to use any mats on hand to fill in designated portions of the matted areas. Using the 3-4 pattern, as many as six continuous longitudinal joints are allowed, compared to only one with a brickwork pattern. A test section was constructed using the 3-4 pattern and trafficked by simulated F-15E and C-17 traffic. The test results showed a reduction in allowable passes of 92 to 96 % when compared to the brickwork pattern for an installation directly over a subgrade with a California Bearing Ratio of 6. Based on these results, the 3-4 pattern is not recommended for runways or high-speed taxiways, nor for soft soil installations.

Contents

Abstract ii

Figures and Tables v

Preface vii

Unit Conversion Factors viii

1 Introduction 1

1.1 Background 1
1.2 Objective and scope 3

2 Experimental Program 4

2.1 Materials 4
2.1.1 AM2 airfield mat 4
2.1.2 High-plasticity clay (CH) subgrade 5
2.2 Test section general description 5
2.3 Test section construction 8
2.3.1 Subgrade construction 9
2.3.2 AM2 strain gauge instrumentation 16
2.3.3 AM2 mat installation 19
2.4 Traffic application 22
2.4.1 F-15E load cart 22
2.4.2 C-17 load cart 24
2.5 Data collection 25
2.5.1 Cross section 26
2.5.2 Loaded cross section 27
2.5.3 Centerline profile 27
2.5.4 Dynamic deflection 27
2.5.5 Borescope observation 28
2.6 Failure criteria 29
2.6.1 Mat breakage 29
2.6.2 Permanent deformation 29

3 Test Results 32

3.1 Mat behavior under traffic (visual observations) 32
3.1.1 F-15E test item 32
3.1.2 C-17 test item 34
3.2 Permanent deformation 36
3.2.1 Centerline profiles 36
3.2.2 Cross sections 36
3.3 Elastic deflection 42
3.4 Strain gauge data 44

4 Analysis of Results 54
4.1 F-15E test item 54
4.1.1 Mat breakage 54
4.1.2 Permanent deformation 55
4.1.3 Elastic deflection 56
4.1.4 Strain gauge readings 56
4.2 C-17 test item 57
4.2.1 Mat breakage 57
4.2.2 Permanent deformation 59
4.2.3 Strain gauge readings 59

5 Conclusions and Recommendations 61
5.1 Conclusions 61
5.2 Recommendations 62

References 63

Appendix: Strain Gauge Data 65

Report Documentation Page

Figures and Tables

Figures

Figure 1. (a) F71 and (b) F72 mat packages. 4
Figure 2. Gradation curve for Vicksburg Buckshot high-plasticity clay (CH). 6
Figure 3. Dry density vs. moisture content for CH subgrade material. 7
Figure 4. CBR vs. moisture content for CH subgrade material. 7
Figure 5. Test section profile. 8
Figure 6. AM2 mat panel layout. 9
Figure 7. Test section excavation. 10
Figure 8. Test pit lined with impervious sheeting. 10
Figure 9. Pulverizing CH. 11
Figure 10. Addition of water to adjust moisture content. 12
Figure 11. Loading processed CH into haul truck. 12
Figure 12. Leveling CH material in test pit prior to compaction. 13
Figure 13. Compacting CH subgrade with pneumatic roller. 13
Figure 14. Nuclear moisture-density gauge test. 14
Figure 15. Field CBR test. 14
Figure 16. Strain gauge locations on the upper underlap and lower overlap regions of AM2 panel end connectors. 17
Figure 17. Typical strain gauge installation on lower overlap region of AM2 panel end connector. 17
Figure 18. Test section instrumentation layout. 18
Figure 19. Insertion of aluminum locking bar between adjacent panels. 19
Figure 20. Installation of AM2 panels on the test section subgrade. 20
Figure 21. Typical Installation of male keylock. 21
Figure 22. Typical final assembled test section. 21
Figure 23. General view of F-15E item. 22
Figure 24. F-15E test load cart. 23
Figure 25. Plan view showing F-15E normally distributed traffic lanes. 23
Figure 26. C-17 test load cart. 24
Figure 27. Plan view showing C-17 normally distributed traffic lanes. 25
Figure 28. Data collection layout for each test item. 26
Figure 29. Surveying unloaded cross section. 27
Figure 30. Surveying loaded cross section. 28
Figure 31. Prism mounted on F-15E load cart. 28
Figure 32. Typical broken upper underlap rail. 33
Figure 33. Six successive panel rail failures where joints were continuous. 33
Figure 34. Layout of failed panels in the F-15E and C-17 items. 34

Figure 35. Typical broken lower overlap rail on C-17 item. 35
Figure 36. Subgrade centerline profile of the F-15E item after 136 passes. 37
Figure 37. Subgrade centerline profile of the C-17 item after 56 passes. 37
Figure 38. Centerline profile on the mat surface of the F-15E item. 38
Figure 39. Centerline profile on the mat surface of the C-17 item. 38
Figure 40. Average deformation on the subgrade of the F-15E item. 39
Figure 41. Average deformation on the subgrade of the C-17 item. 39
Figure 42. Average deformation on the loaded mat surface of the F-15E item. 40
Figure 43. Average deformation on the loaded mat surface of the C-17 item. 40
Figure 44. Average deformation on the unloaded mat surface of the F-15E item. 41
Figure 45. Average deformation on the unloaded mat surface of the C-17 item. 41
Figure 46. Elastic deflection measurements' wander distribution on F-15 item. 43
Figure 47. Elastic deflection elevation distribution on F-15 item. 43
Figure 48. Elastic deflection on F-15 item mat surface at various pass levels. 44
Figure 49. Strain gauge data for F-15E item, SG 62F1, passes 1-10. 45
Figure 50. Strain gauge data for C-17 item, SG 61F2, passes 1-12. 45
Figure 51. Strain gauge data for F-15E item, passes 1-10. 47
Figure 52. Strain gauge data for F-15E item, passes 11-16. 48
Figure 53. Strain gauge data for F-15E item, passes 17-32. 48
Figure 54. Strain gauge data for F-15E item, passes 33-48. 49
Figure 55. Strain gauge data for F-15E item, passes 49-80. 49
Figure 56. Strain gauge data for F-15E item, passes 81-112. 50
Figure 57. Strain gauge data for F-15E item, passes 113-126. 50
Figure 58. Strain gauge data for F-15E item, passes 127-128. 51
Figure 59. Strain gauge data for F-15E item, passes 129-136. 51
Figure 60. Strain gauge data for C-17 item, passes 1-12. 52
Figure 61. Strain gauge data for C-17 item, passes 13-28. 52
Figure 62. Strain gauge data for C-17 item, passes 29-56. 53

Tables

Table 1. Summary of AM2 subgrade sensitivity testing results. 3
Table 2. AM2 mat properties. 5
Table 3. Average in situ properties of the subgrade in each test item. 16
Table 4. Strain gauge installation locations. 18
Table 5. Data collection intervals for F-15E traffic. 25
Table 6. Data collection intervals for the C-17 test item. 26
Table 7. F-15E item mat damage summary. 34
Table 8. C-17 item mat damage summary. 36
Table 9. Maximum measured permanent deformation values for each test item. 42

Preface

This study was conducted for the U.S. Naval Air Systems Command (NAVAIR) Expeditionary Airfield (EAF) team and the U.S. Air Force Civil Engineer Center (AFCEC). Technical oversight was provided by Jeb S. Tingle.

The work was performed by the Airfields and Pavements Branch (GM-A) of the Engineering Systems and Materials Division (GM), U.S. Army Engineer Research and Development Center, Geotechnical and Structures Laboratory (ERDC-GSL). At the time of publication, Dr. Gary L. Anderton was Chief, CEERD-GM-A; Dr. Larry N. Lynch was Chief, CEERD-GM; and Dr. David A. Horner, CEERD-GV-T, was the Technical Director for Force Projection and Maneuver Support. The Deputy Director of ERDC-GSL was Dr. William P. Grogan, and the Director was Dr. David W. Pittman.

COL Jeffrey R. Eckstein was the Commander of ERDC, and Dr. Jeffery P. Holland was the Director.

Unit Conversion Factors

Multiply	By	To Obtain
cubic feet	0.02831685	cubic meters
feet	0.3048	meters
inches	0.0254	meters
kip-inches	112.948	newton-meters
pounds (force)	4.448222	newtons
pounds (force) per square foot	47.88026	pascals
pounds (force) per square inch	6.894757	kilopascals
pounds (mass)	0.45359237	kilograms
square feet	0.09290304	square meters
square inches	6.4516 E-04	square meters

1 Introduction

1.1 Background

AM2 aluminum matting has been the primary temporary airfield matting system used by the U.S. military since the late 1960s. AM2 was developed by the U.S. Navy, but has been adopted for use by the U.S. Air Force (USAF) and U.S. Army for fixed wing and rotary wing operational surfaces. Over the years, AM2 has been modified to address limiting structural concerns. The current production version of AM2 is modification (MOD) 5.

An AM2 surface is comprised of interlocking 2-ft-by-12-ft full panels and 2-ft-by-6-ft half panels that are 1.5 in. thick. The original shipping package, F44, contained 16 12-ft panels and four 6-ft panels. Each package was designed to allow assembly of two 108-ft-wide rows or four 54-ft-wide rows in a brickwork configuration with no continuous longitudinal joints. The brickwork pattern assures maximum load carrying capability of the system. Since 6-ft panels are only used for the row ends, more 12-ft panels are required for assembly. However, ship transportation of the mats across the globe led to a need for the mats to be shipped on an International Organization for Standardization (ISO) flat rack for compatibility with other containerized goods. A decision was made by the U.S. Navy to re-package AM2 into new shipping packages, which resulted in the F71 and F72 shipping configurations.

The F71 contains 18 12-ft mats, and the F72 contains 18 6-ft mats. The new configurations allow one F71 and one F72 to be placed end-to-end on a 20-ft ISO flat rack and optimize use of the available space. The new package configuration also reduces confusion when designing a mat surface. In some instances, F44 packages were re-bundled with different numbers of 6-ft panels inside the 12-ft mat packages. Separating the panels into the F71 and F72 packages eliminates the need to include mixed sizes in packages and improved the accuracy of panel inventories.

The optimization of packaging and shipping of AM2 required equal numbers of 12-ft and 6-ft mat panels to be delivered with each AM2 order. Since only a fraction of the available 6-ft panels are needed to assemble a brickwork pattern, many extra 6-ft panels were unused. To optimize mat use, the Naval Air Systems Command (NAVAIR) Expeditionary Airfield

Team (EAF) created an allowance for two alternate assembly patterns, the 2-1 and the 3-4 lay patterns.

The 2-1 lay pattern was designed for use on all aircraft operating surfaces, including runways and high speed taxiways. The pattern consists of installing AM2 in a brickwork configuration for two rows. The third row is started with a single 12-ft panel and is then filled entirely with 6-ft panels to complete the desired width. The 2-1 lay pattern results in sections with two continuous 2-ft end (longitudinal) joints.

The 3-4 lay pattern was designed only for parking or slow-speed secondary taxi areas and is not allowed for use on runways or high-speed primary taxiways. The 3-4 pattern consists of installing three rows of a brickwork pattern and then four rows of any matting that is available. Under worst-case conditions, the 3-4 pattern can result in as many as six continuous 2-ft end (longitudinal) joints.

Although the two patterns were approved by NAVAIR EAF, they had not been evaluated under simulated aircraft loading conditions to determine if any reduction in the number of allowable passes was caused by the allowance of continuous longitudinal joints. Additionally, NAVAIR developed a Dynamic Interface Model (DIM) to analyze aircraft landing and takeoffs on AM2. The model was validated through laboratory subscale tests, but additional development and validation was required to accurately model the matting subsurface and soil interaction for various installation patterns.

NAVAIR EAF partnered with the Air Force Civil Engineer Support Center (AFCEC) to sponsor the following full-scale traffic evaluations:

1. brickwork pattern,
2. 2-1 pattern,
3. 3-4 pattern,
4. 90-degree traffic application,
5. traffic over a voided subgrade, and
6. in-plane bow and
7. vehicle breaking.

These tests were designed to determine the number of allowable aircraft passes for each pattern and trafficking condition and to gather strain and

soil deformation inputs to feed the DIM. Information from these tests were then compared to evaluations of AM2 assembled in a brickwork pattern over soils with a California Bearing Ratio (CBR) of 6conducted in 2005 and 2006 (Rushing and Tingle 2007; Rushing and Torres 2007). Other AM2 brickwork tests with CBRs of 10, 15, 25, and 100 conducted from 2007 through 2012 were used for analysis (Rushing et al. 2008; Rushing and Mason 2008; Garcia et al. 2014; Garcia et al. in preparation). A summary of the results of the previous tests, in terms of number of passes to failure for a normally distributed traffic pattern, are shown in Table 1.

Table 1. Summary of AM2 subgrade sensitivity testing results.

Sustained Traffic Passes		
Subgrade Strength (CBR)	F-15E	C-17
6	1,500	1,500
10	3,000	6,000
15	4,100	7,000
25	6,300	10,000*
100	23,000	

* Failure was not achieved. Trafficking was stopped because of time constraints.

1.2 Objective and scope

The objectives of the effort described herein were to evaluate the AM2 3-4 lay pattern under simulated F-15E and C-17 aircraft traffic over a subgrade with a CBR of 6, to determine the number of allowable passes, and to record strain and subgrade deformation data needed to calibrate the DIM. To accomplish these objectives, a full-scale test section was constructed with a 36-in.-deep high-plasticity clay (CH) subgrade that had been processed to obtain a CBR of 6. The AM2 mat system was installed in a 3-4 lay pattern directly on the prepared subgrade, and the test section was trafficked using simulated F-15E and C-17 aircraft traffic until pre-defined failure criteria were achieved. The results were compared to those from a previous evaluation of the AM2 brickwork configuration over a CH subgrade with a 6 CBR.

In this report, Chapter 2 includes a description of the AM2 airfield matting system, construction of the full-scale test section, traffic application, data collection, and failure criteria. The results and analyses of the traffic tests are presented in Chapters 3 and 4, respectively. Pertinent conclusions and recommendations are noted in Chapter 5.

2 Experimental Program

The following sections describe the AM2 airfield mat, construction of the full-scale test section, traffic application, data collection, and the failure criteria used to determine test failure.

2.1 Materials

2.1.1 AM2 airfield mat

AM2 airfield mat was developed in the 1960s under a program sponsored by the Naval Air Engineering Center, in Philadelphia, Pennsylvania. Various versions of AM2 were tested under simulated aircraft loads at the U.S. Army Engineer Waterways Experiment Station in Vicksburg, Mississippi, from 1961 through 1971, with major procurements beginning in 1965. The original AM2 mat has been modified through the years to address limiting structural concerns. The current production version of AM2, MOD 5, was obtained from NAVAIR, in Lakehurst, New Jersey. Photos of the AM2 F71 and F72 packages similar to those used in this test are shown in Figure 1.

Figure 1. (a) F71 and (b) F72 mat packages.

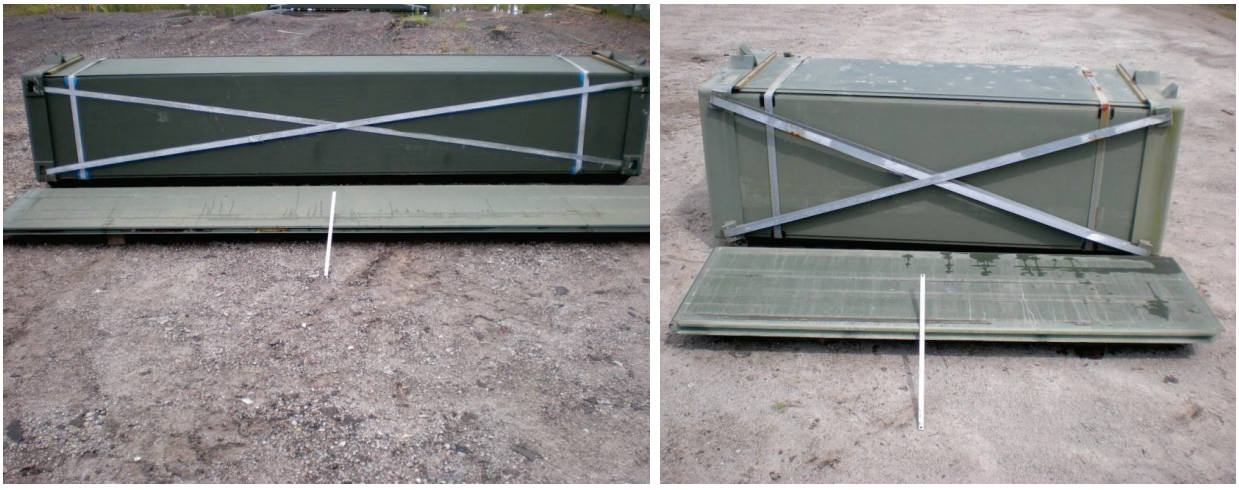

(a) (b)

Pertinent properties of the AM2 mat used in this evaluation are shown in Table 2. Each panel was 2 ft by 12 ft by 1.5 in. and fabricated from a single 6061-T6 aluminum alloy extrusion with end connectors welded to the 2-ft ends to form a complete panel. The core of the extruded panels was comprised of vertical stiffeners spaced 1.75 in. apart in the 12-ft direction.

The mat was also made in half panels to allow a staggered "brickwork" configuration. The panels were joined along the two 12-ft edges by a hinge-type male/female connection. The adjacent 2-ft ends were joined by an overlap/underlap connection secured by an aluminum locking bar. The panels were coated with an anti-skid material to increase the surface friction. The AM2 panels were delivered in F71 and F72 packages and were in unused condition. The panels were visually inspected to ensure that they had not been damaged prior to testing and to make certain they met procurement specifications for AM2 matting.

Table 2. AM2 mat properties.

	Full panel	Half panel
Length (ft)	12	6
Width (ft)	2	2
Thickness (in.)	1.5	1.5
Panel Weight (lbf)	145.5	74.4
Unit Weight (lbf/ft^2)	6.1	6.3

2.1.2 High-plasticity clay (CH) subgrade

The CH material used for subgrade construction was procured from a local source in Vicksburg and was subjected to laboratory tests including grain-size analysis (hydrometer), Atterberg Limits, modified-Proctor compaction, and unsoaked CBR testing. Classification data for the subgrade soil are shown in Figure 2. Moisture-density and CBR-moisture content relationships are shown in Figures 3 and 4, respectively. These data were used to determine the target moisture content and dry density required to obtain the target CBR of 6.

2.2 Test section general description

The traffic tests were conducted on a full-scale test section constructed and trafficked under shelter in the Hangar 4 pavement test facility at the ERDC. AM2 mat panels were placed directly over a 36-in.-deep CH subgrade prepared to a CBR of 6 over an existing silt foundation, as shown in Figure 5. The mat panels were trafficked until failure, as described later in this chapter.

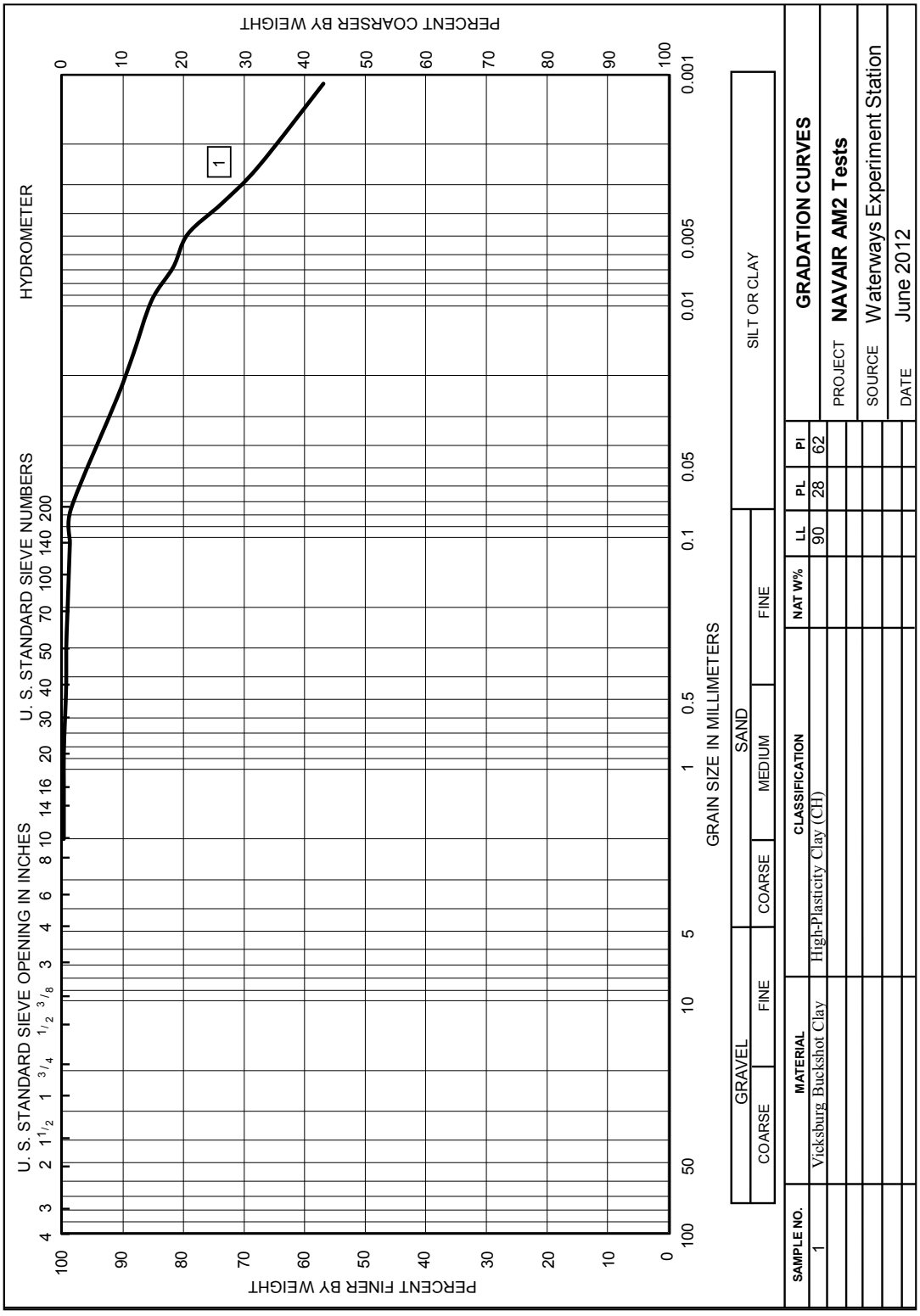

Figure 2. Gradation curve for Vicksburg Buckshot high-plasticity clay (CH).

Figure 3. Dry density vs. moisture content for CH subgrade material.

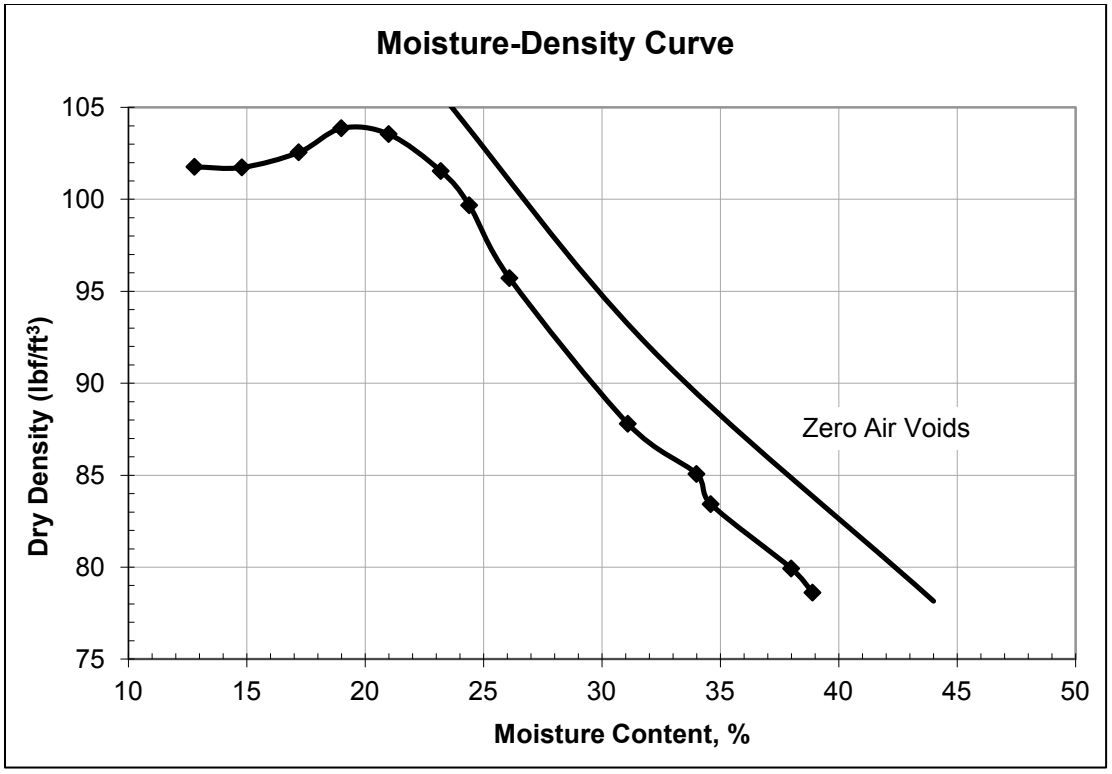

Figure 4. CBR vs. moisture content for CH subgrade material.

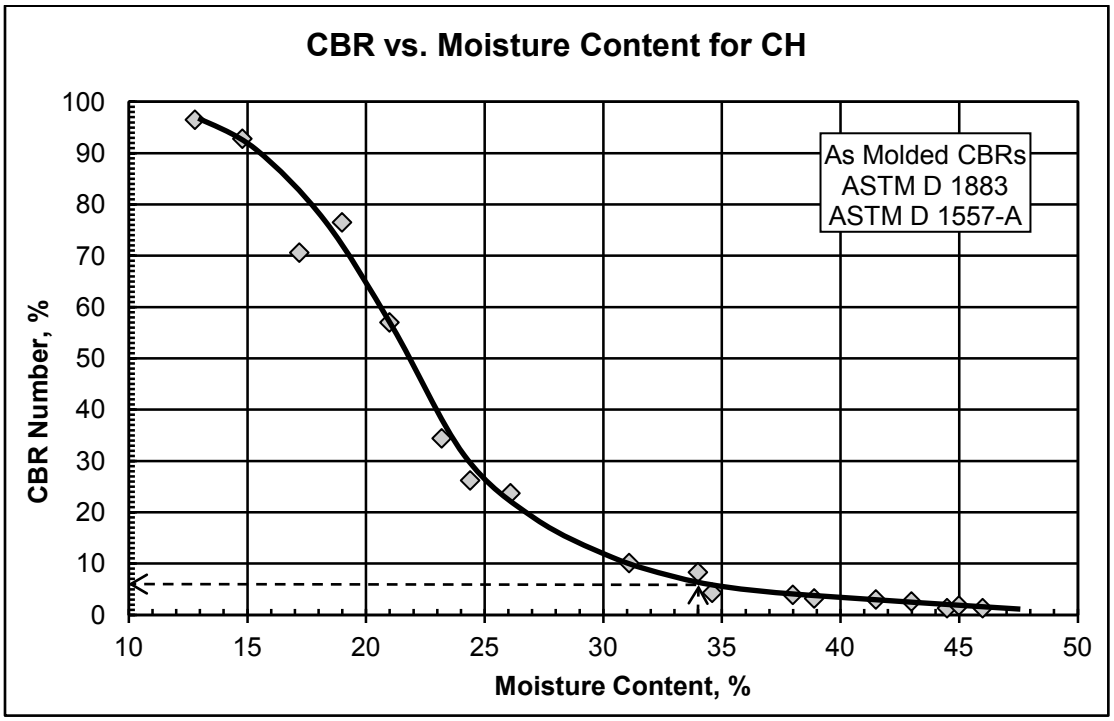

Figure 5. Test section profile.

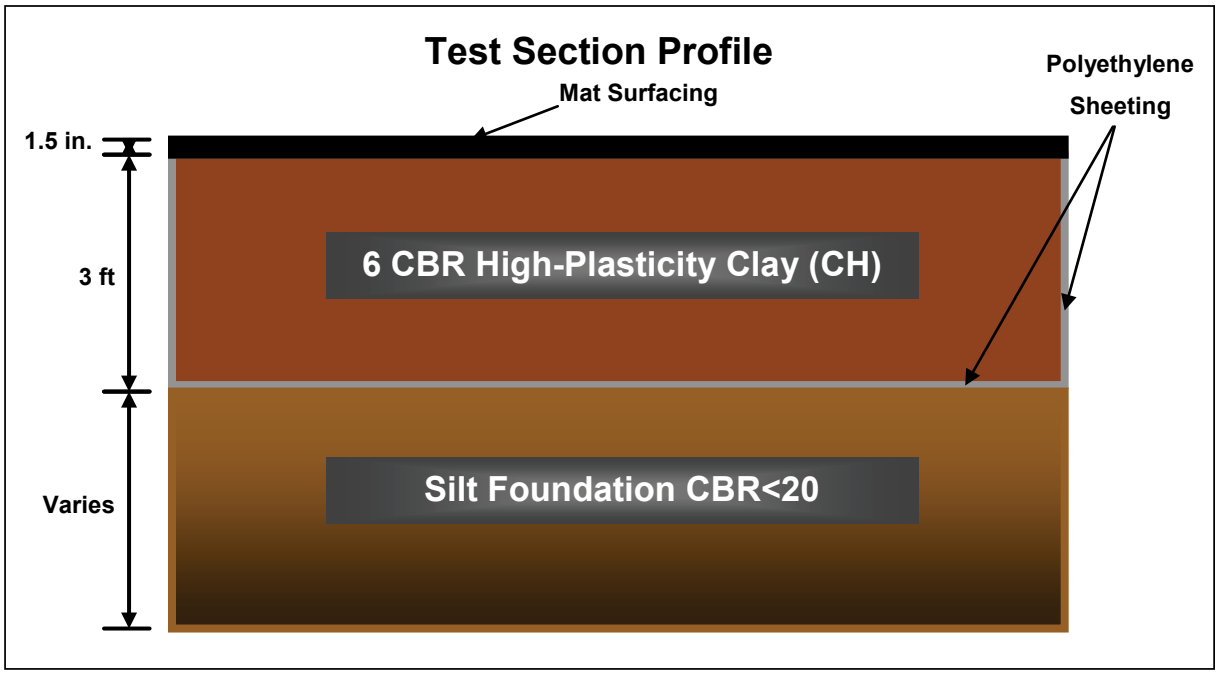

A general layout of the test section, along with panel designations, is shown in Figure 6. Each panel was identified with a number to track damage during trafficking. The test section consisted of a 60-ft-wide-by-42-ft-long section of matting that was subsequently divided into two test items. An area centered 18 ft from the west edge of the test section had a 3.75-ft-wide lane designated for simulated F-15E traffic, and an area centered 18 ft from the east edge had a 9-ft-wide lane designated for simulated C-17 traffic.

Lanes for the F-15E and C-17 items were trafficked according to normally distributed wander patterns associated with the F-15E and C-17 aircrafts, which are described later in this chapter.

2.3 Test section construction

The following sections describe the construction of the foundation subgrade and the AM2 mat installation. Field and laboratory soil testing data used to determine the moisture, density, and bearing capacity in terms of CBR are also included.

Figure 6. AM2 mat panel layout.

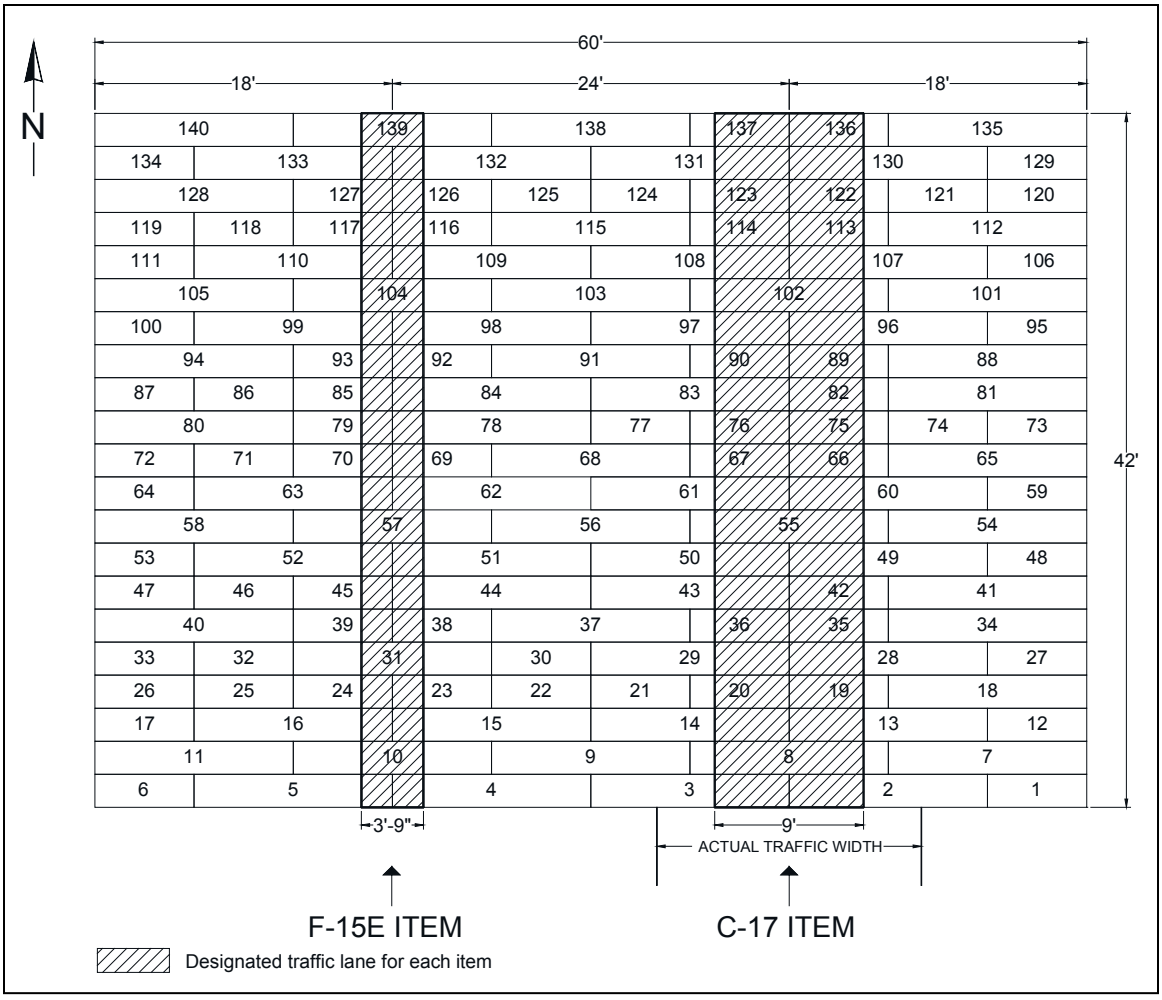

2.3.1 Subgrade construction

The test section subgrade was built using in-place material from the "Opposite Lay" test section previously constructed to a CBR of 6. The original subgrade was constructed by excavating a 60-ft-wide-by-42-ft-long test pit to a minimum 36-in. depth below the existing finished grade in Hangar 4, as shown in Figure 7. The soil at the bottom of the excavation was a silt material (ML) having a CBR less than 20. The existing ML material was leveled with a bulldozer and compacted with a pneumatic roller and a vibratory steel-wheel compactor to ensure that the remainder of the test section was constructed over a stable foundation. The bottom and sides of the test pit were lined with impervious 6-mil polyethylene sheeting to minimize moisture migration from the 36 in. of new CH soil serving as the test section subgrade, as shown in Figure 8.

Figure 7. Test section excavation.

Figure 8. Test pit lined with impervious sheeting.

The CH was processed at a nearby preparatory site by spreading the material to a uniform 12-in. depth, pulverizing the material with a rotary mixer, adjusting the moisture content, pulverizing the material again, and stockpiling it as shown in Figures 9 through 11. This was an iterative process necessary to achieve a uniform distribution of moisture throughout the material. Once the CH had been processed to the target moisture content, it was placed in the test section, spread by a bulldozer in 8-in. lifts, and compacted with a pneumatic roller to a depth of 6 in., as shown in Figures 12 and 13.

Each compacted lift was subjected to nuclear moisture/density tests (ASTM D 6938), as shown in Figure 14, in addition to convection oven moisture determination tests (ASTM D4643), to verify that target values had been met. In situ CBR tests (CRD-C 654-95), as shown in Figure 15, were conducted at the north and south locations of each test item on every 6-in. compacted lift to verify that the target CBR of 6 had been reasonably achieved. If the average pretest CBR of a lift differed from the target value by more than +1.0 or -0.5 CBR, the lift was reconstituted. Each lift was surveyed to obtain an average thickness. After data collection, the surface was scarified an average depth of 1 in. with a rotary mixer prior to placement of the following lift to facilitate bonding at the interface.

Figure 9. Pulverizing CH.

Figure 10. Addition of water to adjust moisture content.

Figure 11. Loading processed CH into haul truck.

Figure 12. Leveling CH material in test pit prior to compaction.

Figure 13. Compacting CH subgrade with pneumatic roller.

Figure 14. Nuclear moisture-density gauge test.

Figure 15. Field CBR test.

For the 3-4 lay pattern test section, the upper 12 in. of the existing test section were removed and reprocessed using the procedures described above. Field CBR tests indicated that the existing material from 12 in. to 36 in. retained a CBR of approximately 6; therefore, reconstruction of the entire depth was unnecessary. The reprocessed material was replaced in two 6-in. lifts. Field CBR tests were again performed on each lift as described above to ensure the target CBR of 6 was achieved.

The results of the CBR, moisture, and density tests during construction (pretest) and after trafficking (posttest) for both test items are shown in Table 3. The posttest in situ CBR, moisture, and density measurements were used to determine the depth of subgrade that might have undergone gradual drying and possible densification under traffic. Some increase in CBR was expected because of thixotropic properties of clay structures and gradual drying and densification during trafficking. Based on historic testing data (Rushing and Tingle 2007; Rushing and Torres 2007; Rushing et al. 2011; Garcia et al. 2012; Rushing et al. 2012) , surface increases of less than 5 CBR and increases of less than 3 CBR at a depth of 6 in. are common and, therefore, acceptable.

The moisture content and density measurements presented in Table 3 generally follow the trends found in laboratory measurements presented in Figures 3 and 4. However, previous experience has shown that the field moisture content required to construct a CBR of 6 typically ranges from 30% to 32% instead of 34% as suggested in Figure 4.

For the F-15E test item, the posttest CBR measurements at the surface increased from 5.7 to 6.4 during the trafficking. A 6-in. pit was excavated, and another field CBR test was conducted. The CBR at the bottom of the pit showed an increase from 6.0 to 6.6. Since both the surface and 6-in. measurements were within historic ranges and were still within the construction tolerance of 5.5 to 7.0, the strength of the subgrade remained within acceptable limits throughout testing.

For the C-17 test item, the posttest CBR measurements at the surface and at the bottom of the 6-in. pit increased from 6.1 to 6.4 and from 6.2 to 6.9, respectively. At both locations, the change was within historically acceptable ranges and was still within the initial construction tolerance. Therefore, the strength of the subgrade remained within acceptable limits throughout testing.

Table 3. Average in situ properties of the subgrade in each test item.

Test Depth	Wet Density [1] (lbf/ft³)	Dry Density [1] (lbf/ft³)	Moisture [1] (%)	Oven Moisture (%)	In Situ CBR (%)	Change in CBR (%)
Pre-Test F-15E Item						
Surface	116.0	85.0	36.6	30.9	5.7	-
6 in.	125.2	93.4	34.6	31.3	6.0	-
12 in.	118.8	92.3	28.7	29.1	6.2	-
18 in.	118.1	91.4	29.3	31.3	6.1	-
24 in.	116.3	87.6	32.7	27.2	5.7	-
30 in.	117.5	88.9	32.0	32.6	6.2	-
Post-Test F-15E Item						
Surface	119.7	89.5	33.8	29.8	6.4	+0.7
6 in.				32.6	6.6	+0.6
Pre-Test C-17 Item						
Surface	117.3	86.9	34.9	31.4	6.1	-
6 in.	117.7	87.6	34.1	30.4	6.2	-
12 in.	116.1	88.7	30.8	32.2	5.8	-
18 in.	117.1	90.1	29.9	30.8	6.0	-
24 in.	115.1	88.5	30.2	27.5	5.9	-
30 in.	115.2	86.9	32.7	33.2	6.1	-
Post-Test C-17 Item						
Surface	118.6	87.6	35.4	31.7	6.4	+0.3
6 in.				32.0	6.9	+0.7

[1] Readings are from nuclear density gauge.

2.3.2 AM2 strain gauge instrumentation

Prior to installation, 24 individual mat panels were instrumented with a total of 56 foil strain gauges on the upper underlap and lower overlap regions of the 2-ft end connectors as shown in Figures 16 and 17. The gauges were installed by the Applied Research Laboratory (ARL) at Pennsylvania State University (PSU) under a contract with NAVAIR. The gauged mats were delivered to the ERDC for this evaluation. The locations of gauged panels in the test array are shown in Figure 18, and the number and location of gauges installed on each panel are detailed in Table 4.

The strain gauges were used to gather critical strain information to feed the DIM developed by NAVAIR. The DIM showed the installation regions on the prongs to be the component most susceptible to breaking. The measured strain results were used to validate the values predicted by the DIM for the 3-4 lay pattern. The gauged end connectors were placed along

the centerline of both items to measure the maximum strains induced under simulated aircraft traffic loads. Data points were collected at a rate of 100 Hz with the Campbell Scientific® CR5000 measurement and data logger system operated by an experienced instrumentation technician.

Figure 16. Strain gauge locations on the upper underlap and lower overlap regions of AM2 panel end connectors.

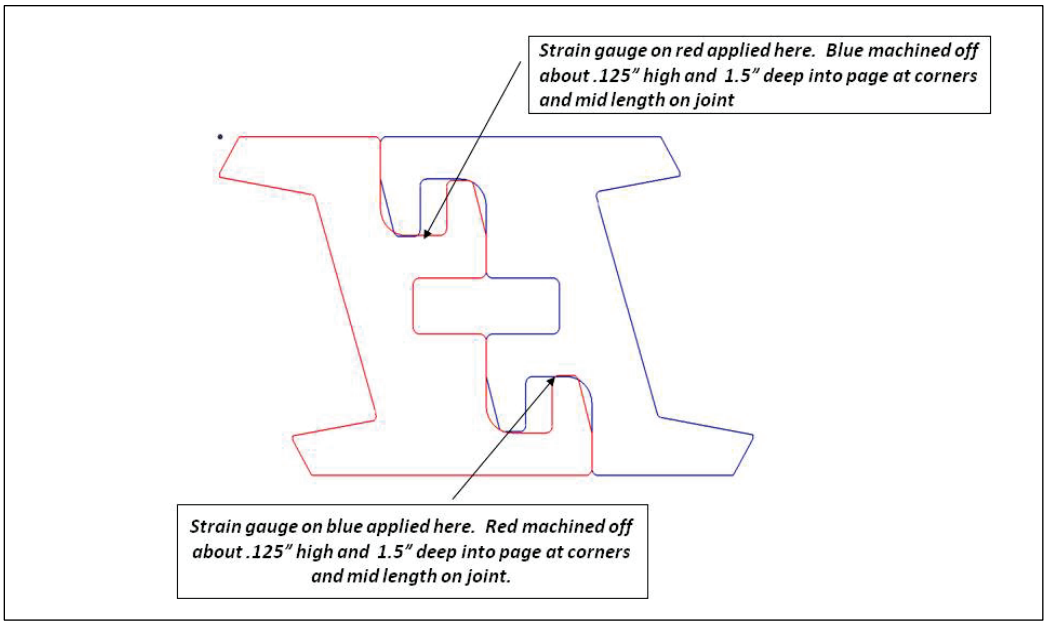

Figure 17. Typical strain gauge installation on lower overlap region of AM2 panel end connector.

Figure 18. Test section instrumentation layout.

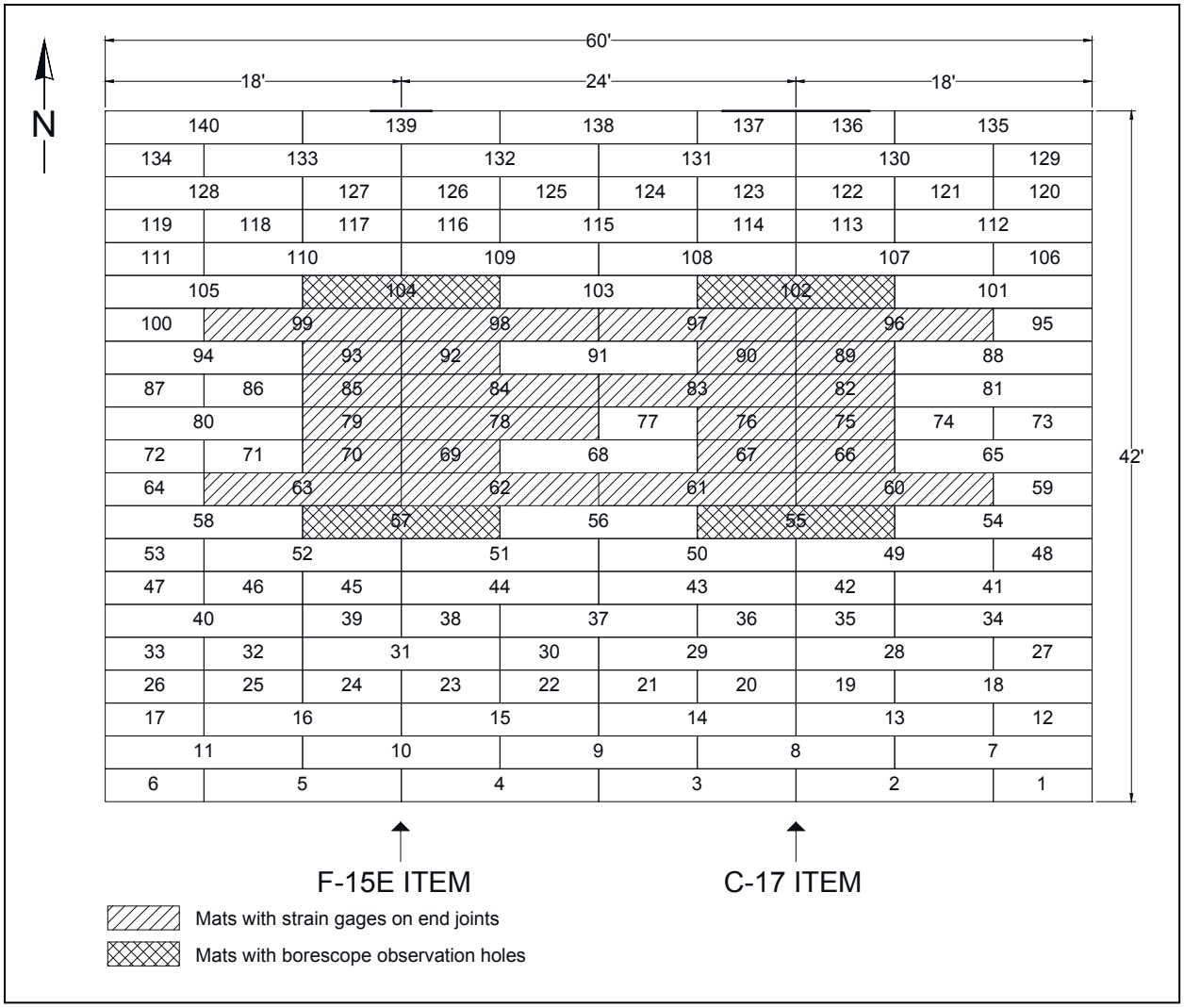

Table 4. Strain gauge installation locations.

Gauge Installation location	12-ft panel lower overlap	12-ft panel upper underlap	6-ft panel lower overlap	6-ft panel upper underlap
Panel Number (gauge count)	99 (2)	98 (2)	93 (2)	92 (2)
	63 (2)	84 (3)	85 (3)	69 (2)
	97 (2)	78 (3)	79 (3)	89 (2)
	83 (3)	62 (2)	70 (2)	82 (3)
	61 (2)	96 (2)	90 (2)	75 (3)
		60 (2)	76 (3)	66 (2)
			67 (2)	

2.3.3 AM2 mat installation

The AM2 airfield mat system was placed on the surface of the prepared test section subgrade by an experienced labor crew. The mat bundles were placed on the test section with a forklift, and the individual panels were carried by two men and placed into position.

The first mat panel was placed flat on the ground with the long dimensions perpendicular to the direction of traffic and with the male hinge connector facing north. The second panel was positioned adjacent to the 2-ft end of the first, allowing the overlapping end connector of the second panel to drop into position over the underlapping end connector of the first panel. A rectangular slot was formed between the two end connector rails, and an aluminum locking bar was inserted into the slot, as shown in Figure 19. This locking bar prevented the ends of the mat panels from separating. This process was continued until the first row was installed.

Figure 19. Insertion of aluminum locking bar between adjacent panels.

For the second row, the 12-ft female hinge connector was attached to the male hinge connector of panels from the first row, and the panel was pivoted into place, as shown in Figure 20. The next panel was installed by attaching the female hinge connector to the male hinge connector of panels in the first row and allowing the overlapping end connector rail to

pivot over and connect to the underlapping end connector rail of the adjacent panel. An aluminum locking bar was inserted into the space provided to keep the panels from separating. This process was repeated until the entire mat test section was assembled in the 3-4 configuration as shown in Figure 6.

Figure 20. Installation of AM2 panels on the test section subgrade.

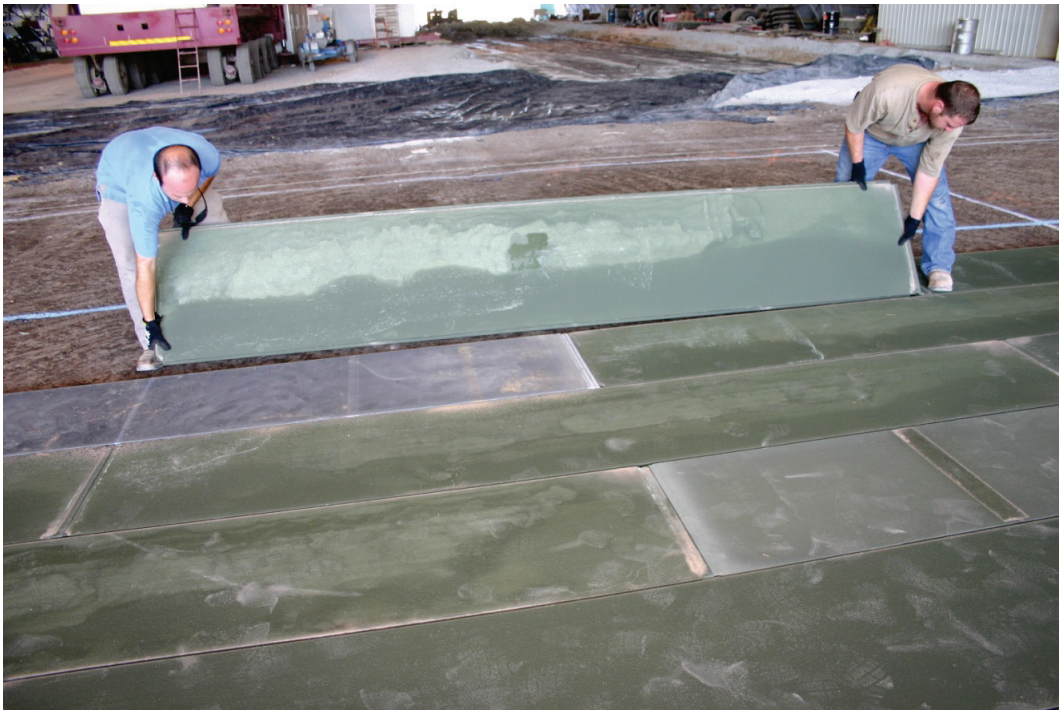

Once assembly was complete, full panels of AM2 were installed along the ends of the traffic lanes to facilitate the entrance and exit of the test vehicles. Male keylocks were attached to the female hinge connector of the panels in the first row to facilitate ramp installation, as shown in Figure 21. A photo of the final assembled test section is shown in Figure 22. Once the mats had been installed, 1,000-lb lead weights were placed along the edges of the test section to anchor the mats and simulate the resistance to movement provided by a large expanse of matting. A general view of the F-15E test item is shown in Figure 23.

Figure 21. Typical Installation of male keylock.

Figure 22. Typical final assembled test section.

Figure 23. General view of F-15E item.

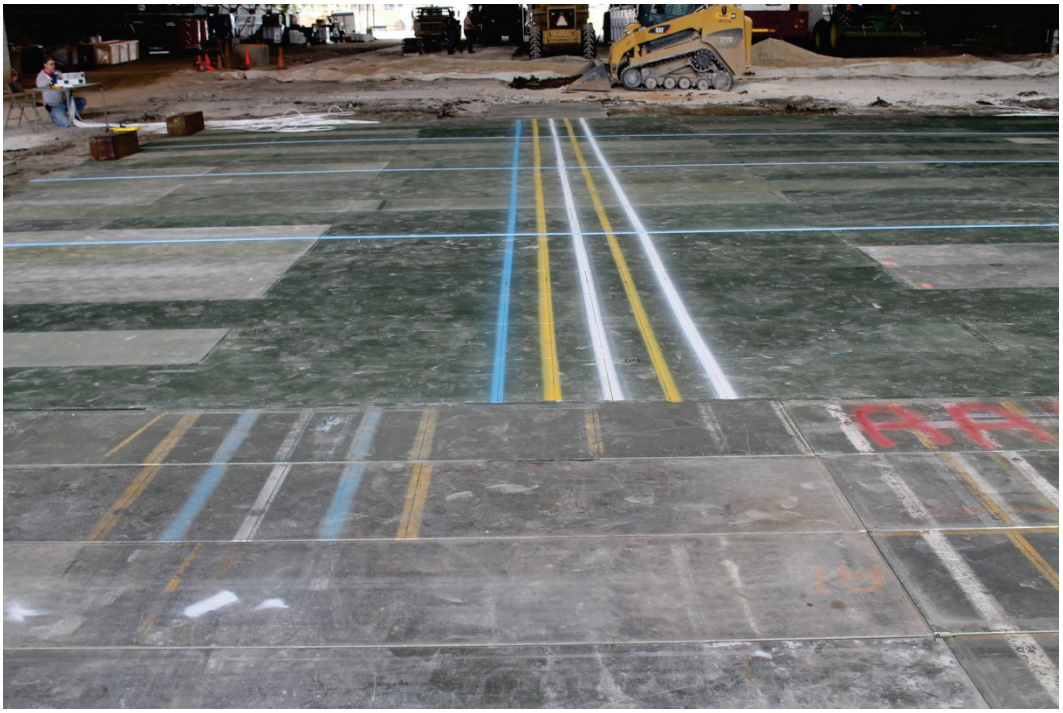

2.4 Traffic application

This section describes the application of simulated aircraft traffic on the AM2 airfield mat system. Pertinent data concerning the test load carts and application of traffic are provided.

2.4.1 F-15E load cart

A specially designed single-wheel load cart was used to simulate F-15E aircraft traffic. The load cart was equipped with a 36-in.-by-11-in., 30-ply tire inflated to 325 lbf/in.^{2} and loaded such that the test wheel was supporting 35,235 lb. The F-15E load cart was equipped with two outrigger wheels to prevent overturning and was powered by the prime mover of a case vibratory steel-wheel roller as shown in Figure 24.

A normally distributed pattern of simulated traffic was applied in a 3.75-ft-wide traffic area for the F-15E test item, as shown in Figure 25. The traffic area was broken into five lanes that were designed to simulate the traffic distribution pattern, or wander width, of the main landing gear wheel on a mat surface when taxiing to and from an active runway. The width of each lane corresponded to the measured contact width, 9 in., of the F-15E tire when fully loaded and not the overall published tire width of 11 in. The normally distributed traffic patterns were simplified for ease-of-use by the

load cart operator. Traffic was applied by driving the load cart forward and then backward over the length of the test item, then shifting the path of the load cart laterally approximately one tire width on each forward path. This procedure was continued until one pattern of traffic was completed. One pattern resulted in 16 passes, or four coverages. Traffic was continued in this manner until failure of either the mat or the subgrade in the test item occurred. Performance data, both static and dynamic, were collected, and the mat surface was inspected for damage periodically during trafficking.

Figure 24. F-15E test load cart.

Figure 25. Plan view showing F-15E normally distributed traffic lanes.

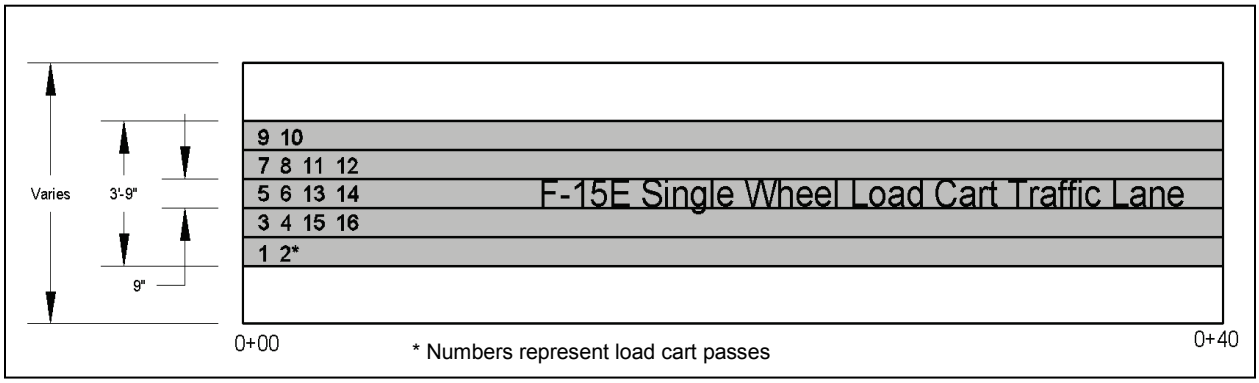

2.4.2 C-17 load cart

The multiple-wheel C-17 load cart was designed to exactly match one full main gear of a C-17 aircraft. The multiple-wheel C-17 load cart was equipped with six 50-in.-by-21-in., 20-ply tires inflated to 142 lbf/in.^{2} and loaded such that the test gear was supporting 269,560 lb, with estimated individual wheel loads of 44,930 lb. The test cart was powered by the front half of a Fiat scraper as shown in Figure 26.

Figure 26. C-17 test load cart.

A simulated normally distributed traffic pattern was applied in a 9-ft-wide traffic area for the C-17 test item, as shown in Figure 27. The traffic areas were divided into individual lanes designed to simulate the traffic distribution pattern, or wander width, of the main landing gear wheels on a mat surface when taxiing to and from an active runway. The width of each lane corresponded to the measured contact width, 18 in., of the C-17 tires when fully loaded and not the overall published tire width of 21 in. The normally distributed traffic patterns were simplified for ease-of-use by the load cart operator. Traffic was applied by driving the load cart forward and then backward over the length of the C-17 test item, then shifting the path of the load cart laterally approximately one tire width on each forward pass. Tracking guides were attached to assist the driver in shifting the load cart the proper amount for each forward pass. This procedure was continued until one pattern of traffic was completed. For the C-17 test item, one pattern resulted in 28 passes, or 25 coverages.

Figure 27. Plan view showing C-17 normally distributed traffic lanes.

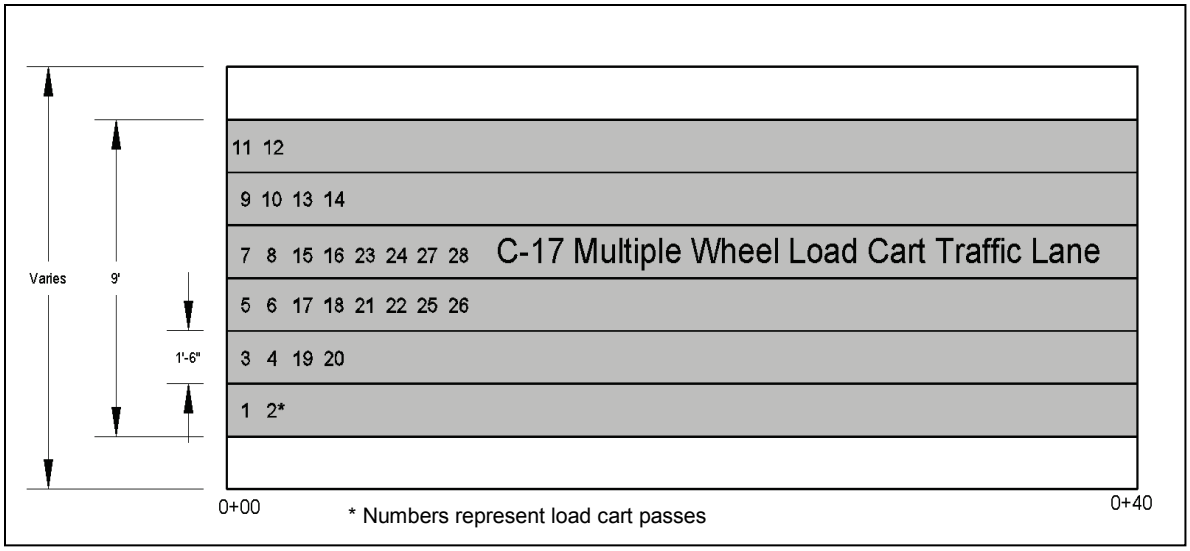

Traffic was continued in this manner until failure, either of the mat or the subgrade, occurred in the test item. Performance data, both static and dynamic, were collected, and the mat surface was inspected for damage periodically during trafficking.

2.5 Data collection

Data collection during trafficking included robotic total station measurements of cross sections, centerline profiles, dynamic elastic deflections, and dynamic strain measurements. The dynamic elastic deflection was collected during the first 16 passes of each traffic interval shown in Tables 5 and 6, and the dynamic strain data were collected for every pass.

Table 5. Data collection intervals for F-15E traffic.

Total Passes	Profile	Unloaded Cross sections	Loaded Cross sections	Dynamic Deflection	Strain Gauges [1]
Pre-Test Subgrade	X	X			
0	X	X	X	X	X
10	X	X	X	X	X
16	X	X	X	X	X
32	X	X	X	X	X
48	X	X	X	X	X
112	X	X	X	X	X
136	X	X	X	X	X
Post-Test Subgrade	X	X			

[1]Strain gauge data were collected continuously.

Table 6. Data collection intervals for the C-17 test item.

Total Passes	Profile	Unloaded Cross Sections	Loaded Cross Sections	Strain Gauges
Pre-Test Subgrade	X	X		
0	X	X	X	X
12	X	X	X	X
28	X	X	X	X
56	X	X	X	X
Post-Test Subgrade	X	X		

2.5.1 Cross section

The data collected prior to, at scheduled pass levels during, and after trafficking were collected at the locations labeled A1, A2, and A3 and along the centerlines, as shown in Figure 28. The locations of perpendicular lines A1, A2, and A3 were selected near the quarter-points of the test items to characterize the average performance while avoiding potential end effects associated with boundary conditions at the ends of the test sections. The location of A2 was chosen in the center of the six continuous end joints, where the maximum deformation was expected to occur. Robotic total station elevation data collected at 1-ft intervals along these lines are called "cross sections" in this report (Figure 29).

Figure 28. Data collection layout for each test item.

Figure 29. Surveying unloaded cross section.

2.5.2 Loaded cross section

In an attempt to measure the permanent deformation of the subgrade underneath the mat surface, a forklift carrying lead weights was parked adjacent to each cross section, and elevation data were once again recorded (Figure 30). These data are noted as “loaded cross sections” in this report.

2.5.3 Centerline profile

Robotic total station elevation data collected at 1-ft intervals along the traffic centerline are labeled “centerline profiles” in this report.

2.5.4 Dynamic deflection

Dynamic elastic deflection data were collected by mounting a survey prism just above the load wheel on the F-15E load cart, as shown in Figure 31, during the first 16 passes of each data collection interval. The robotic total station recorded elevation measurements for every 6 in. of forward or backward movement of the load cart to determine the total deflection occurring in the subgrade and matting system caused by the applied load. The amount of mat damage and the mode of failure were recorded during the traffic phase.

Figure 30. Surveying loaded cross section.

Figure 31. Prism mounted on F-15E load cart.

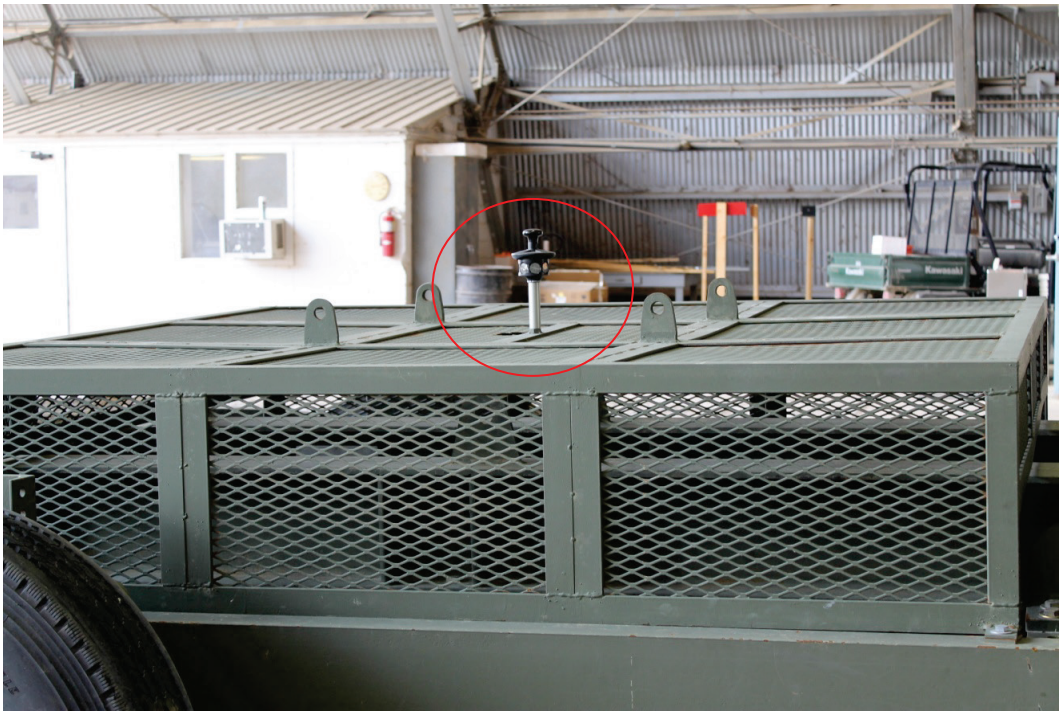

2.5.5 Borescope observation

Observation holes were installed in panels 55, 57, 102, and 104 in an attempt to monitor the deformation progression of the subgrade

underneath the mats. Concentric circles were drawn on the underside of these panels with radii of 3, 6, and 9 in., and two flexible tapes were laid orthogonally across the subgrade to assist in scaling during video review. Panel locations are shown in Figure 18. Videos of the borescope observations have been retained for archiving, but no measurements are reported in this document.

2.6 Failure criteria

The failure criteria established were either (1) 10% mat breakage or (2) the development of 1.25 in. of permanent surface deformation for the F-15E or 3.0 in. of permanent surface deformation for the C-17. These failure criteria were developed based upon previous testing of airfield matting and USAF requirements. Failure criteria values were recorded and monitored for compliance.

2.6.1 Mat breakage

Mat breakage percentages were calculated by dividing the area of the failed panel (or half panel) by the total area influenced by the simulated traffic application in the assembled test item. For example, the total area influenced by the F-15E item was 1,008 ft^2 (24 ft by 42 ft). Ten percent of this area is 101 ft^2, which is equal to the area of 4.2 12-ft panels (5 failures required to exceed criterion). Individual panels were considered failed if observed damage posed a significant tire hazard or caused instability of the load cart. Tire hazards were defined as damage that could not be reasonably maintained by simple field-maintenance procedures. A typical example was a top skin tear in excess of 10 to 12 in., representing significant structural damage to the surface skin with sharp edges that could endanger an aircraft tire.

2.6.2 Permanent deformation

The permanent surface deformation limits of 1.25 in. and 3.0 in. are based on roughness limitations for the F-15E and C-17 aircrafts, respectively. An abrupt change in elevation or the development of a rut in the wheel path greater than the allowable values may exceed roughness limits. The rut depth limit is required since many connecting taxiways and aprons intersect at 90 deg, and crossing perpendicular to a pre-formed rut may cause an abrupt change in elevation, exceeding aircraft limits. Failure by permanent surface deformation was determined from robotic total station elevation

measurements of cross sections and centerline profiles. Each of the following data collection categories were analyzed for compliance with the failure criterion:

1. centerline profile deformation,
2. loaded surface deformation, and
3. unloaded surface deformation

2.6.2.1 Centerline profile deformation

Centerline profile deformation was measured by robotic total station elevation recordings along the traffic centerline. The difference in elevation one or two stations apart (1 or 2 ft apart) was analyzed from plots of the data to determine if an abrupt change in elevation reached failure limits for each interval during trafficking.

2.6.2.2 Loaded surface deformation

An attempt was made to measure the permanent deformation of the subgrade underneath the mat surface by parking a forklift carrying lead weights adjacent to the data collection locations shown in Figure 28 and recording the elevation along these lines. The wheel load applied was approximately 6,000 lb. The goal of the load application was to deflect the mat enough to contact the subgrade but not so much as to induce elastic deflections in the subgrade. However, since the panels' surfaces contained no visual access points, the extent of deflection and location of the subgrade surface were unknown.

The maximum deformation at each location was determined as the difference in elevation from the average height of the elevated material on each side of the trough to the deepest point in the bottom of the trough. Measurements were averaged to obtain a single value for comparison to the failure criterion. The deformation measurements determined by this method are noted as "loaded cross sections" in this report.

2.6.2.3 Unloaded surface deformation

Unloaded surface deformation values were determined from robotic total station elevation measurements along the three cross-section locations shown in Figure 28. The maximum deformation at each location was determined as the difference in elevation from the average height of the

elevated material on each side of the trough to the deepest point in the bottom of the trough. Measurements were averaged to obtain a single value for comparison to the failure criterion. The deformation measurements determined by this method are noted as “unloaded cross sections” in this report.

3 Test Results

3.1 Mat behavior under traffic (visual observations)

The following sections describe all mat breakage and the behavior of the AM2 airfield mat under simulated F-15E and C-17 traffic. A general view of the test section prior to trafficking is shown in Figure 22.

3.1.1 F-15E test item

Trafficking of the F-15E test item began on May 9, 2013. During the first 50 passes, significant bow-wave movement was observed in the region of instrumented panels where six consecutive longitudinal joints were installed. No mat panel damage was observed until the upper underlap of the end connector on Panel 62 separated from the mat after 62 passes, as shown in Figure 32. At this point, Panel 62 was failed. Trafficking was continued. After 69 passes, the upper underlap separated from Panel 69, and it was failed. The same failure mechanism was observed in Panel 78 after 71 passes. All three of these panels were installed consecutively, and the failures were successive. The failures continued to progress, and Panel 84 failed by a broken upper underlap after 120 passes; Panels 92 and 98 were noted to have failed after 135 passes. Since there was no support along the traffic centerline for 12 ft of test section length along these failed panels, trafficking was stopped after 136 passes, and testing on the F-15E item was concluded.

Figure 33 shows the successive panel failures along the centerline with a forklift parked on the surface. At this point in the test, four 12-ft panels and two 6-ft panels had failed, equaling 12% of the test item. Therefore, the test item failed due to mat breakage, and trafficking was terminated to prevent instability of the load cart and damage to the aircraft tire.

When the panels were removed after trafficking was completed, no significant additional damage was noted that could not be observed from the surface. Table 7 gives a summary of mat distresses, permanent surface deformation, and failures on the mat surface at various pass levels for the F-15E item. Figure 34 shows the layout of failed panels for the F-15E item after trafficking concluded.

Figure 32. Typical broken upper underlap rail.

Figure 33. Six successive panel rail failures where joints were continuous.

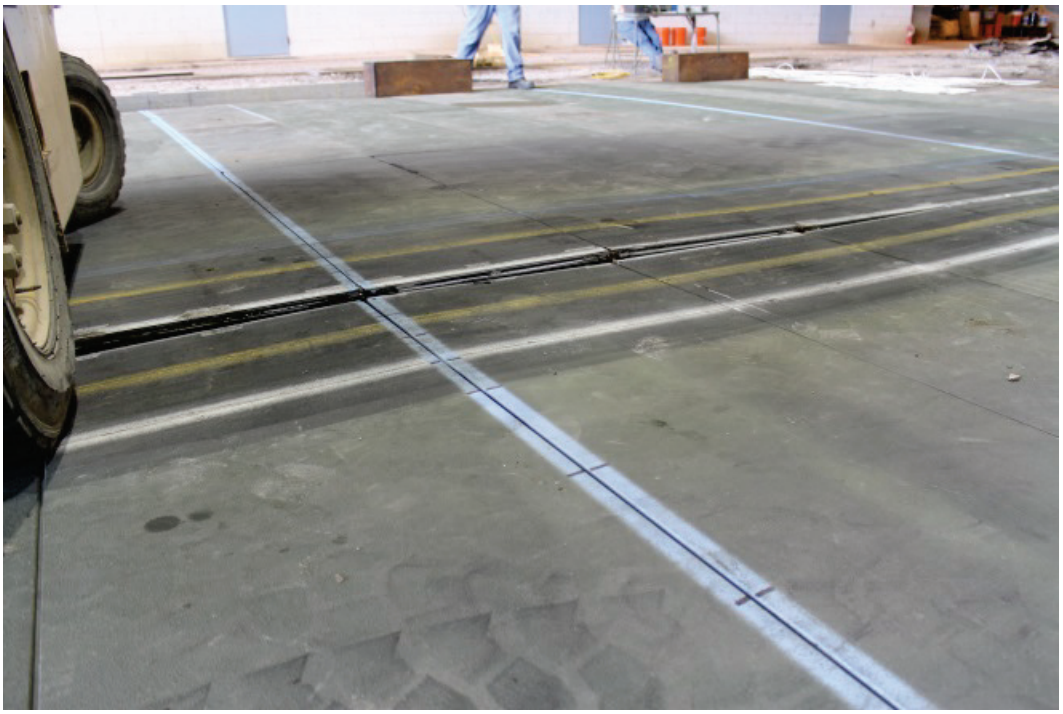

Table 7. F-15E item mat damage summary.

F-15E Passes	Failure Type	Damage Description	Cumulative Failed Panels	Cumulative Percent Mat Failure	Panel Number
62	Mat breakage	Broken upper underlap	1	3%	62
69	Mat breakage	Broken upper underlap	2	4%	69
71	Mat breakage	Broken upper underlap	3	6%	78
120	Mat breakage	Top skin tear	4	9%	84
135	Mat breakage	Broken upper underlap	6	12%	92, 98
		Test item failed by mat breakage			

Figure 34. Layout of failed panels in the F-15E and C-17 items.

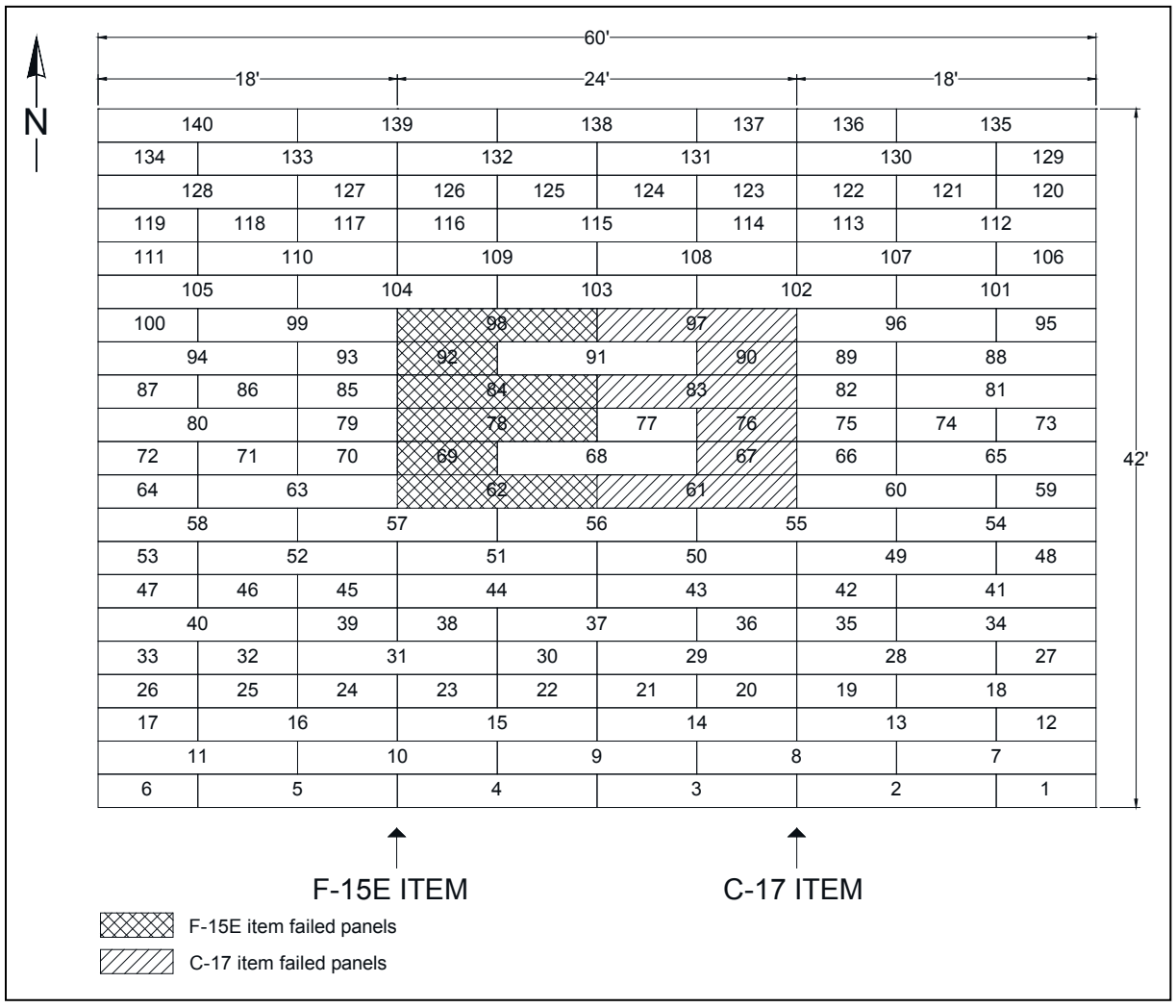

3.1.2 C-17 test item

Trafficking of the C-17 test item over a subgrade with a CBR of 6 began on May 13, 2013. Instrumented panels began to fail quickly along the area with six continuous longitudinal joints. After 28 passes, the lower overlap

broke free from Panel 90, as shown in Figure 35, causing a tire hazard, thus failing the panel. The lower overlap broke from Panel 83 after 46 passes. The trend continued, and the lower overlaps broke from Panels 61, 67, and 76 after 50 passes. When 56 passes were completed, trafficking was stopped, because the failed panels had become a serious threat to the aircraft tires of the test vehicle. The mats were completely separating along the failed joints and were embedding into the subgrade beneath them. Even though the 10% mat breakage failure criteria had not been reached, the section was no longer usable, and total failure was eminent.

Figure 35. Typical broken lower overlap rail on C-17 item.

Upon removal of the panels from the test section, the lower overlap of Panel 97 was also broken, and the panel was failed. The only other damage was a small corner curl in the southwest corner of Panel 96. The non-instrumented panels, 14, 20, 29, 36, 43, and 50, installed in a similar arrangement as the failed panels were not damaged. Table 8 gives a summary of mat distresses, permanent surface deformation, and failures on the mat surface at various pass levels for the C-17 item. Figure 34 shows the layout of failed panels for the C-17 item after trafficking concluded.

Table 8. C-17 item mat damage summary.

F-15E Passes	Failure Type	Damage Description	Cumulative Failed Panels	Cumulative Percent Mat Failure	Panel Number
28	Mat breakage	Broken lower overlap	1	1%	90
46	Mat breakage	Broken lower overlap	2	3%	83
50	Mat breakage	Broken lower overlap	5	6%	61,67,76
56	Mat breakage	Broken lower overlap	6	8%	97

3.2 Permanent deformation

Permanent deformation was measured in each test item on the subgrade before and after the test, on the mat surface before trafficking, at intervals during trafficking shown in Tables 5 and 6, and on the mat surface after trafficking was concluded. To show only the changes that occurred because of trafficking, the pre-traffic data were subtracted from all subsequent data collected after trafficking began to normalize the data. The discussions that follow are based on normalized data.

3.2.1 Centerline profiles

Plots of the centerline profile data, as determined from robotic total station recordings, for the F-15E and C-17 test items are shown in Figures 36 through 39. Maximum abrupt changes in elevation were determined by observing the difference in elevation of data points within two stations of each other and choosing the maximum value for each plot. Each maximum value was then used for comparison to the roughness criterion.

3.2.2 Cross sections

Plots of the average cross-section elevation data, collected along lines A1, A2, and A3 shown in Figure 28 for each test item, are shown in Figures 40 through 45. Maximum deformation values for the subgrade, loaded, and unloaded cross sections were determined as the difference in elevation from the average height of the elevated material on each side of the trough to the deepest point in the bottom of the trough. Table 9 summarizes maximum deformation values measured on each item for profiles and cross sections.

Figure 36. Subgrade centerline profile of the F-15E item after 136 passes.

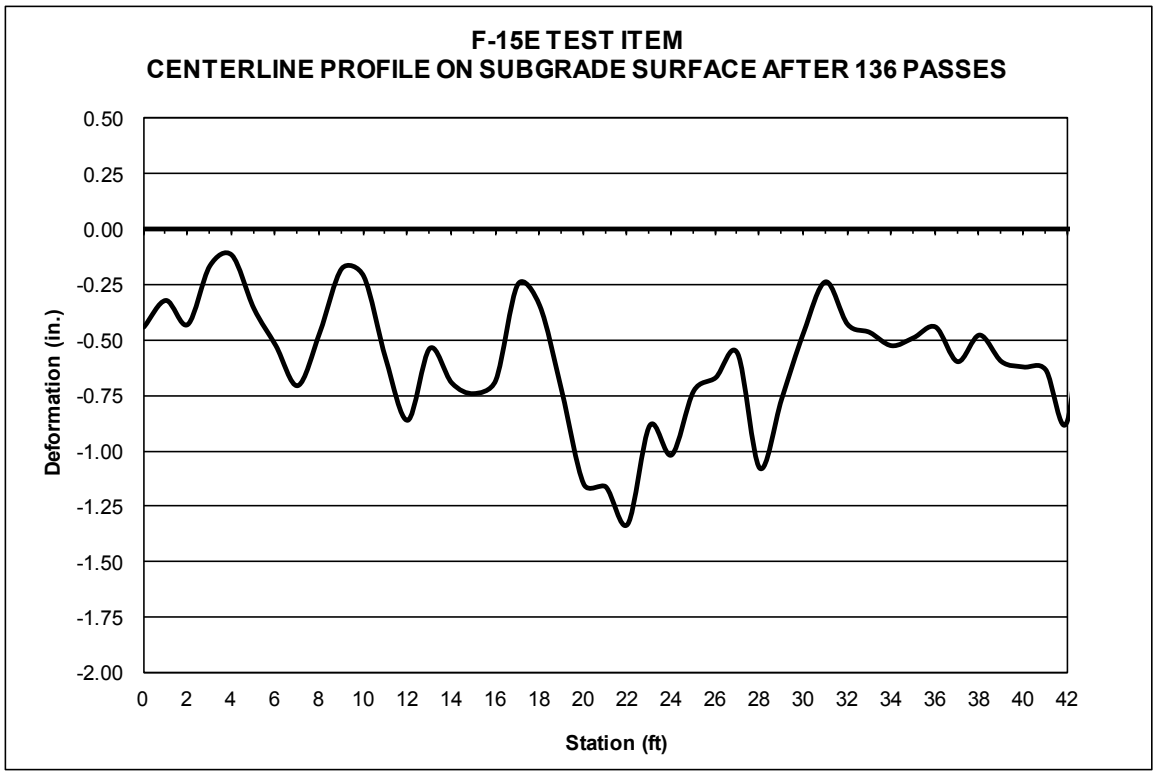

Figure 37. Subgrade centerline profile of the C-17 item after 56 passes.

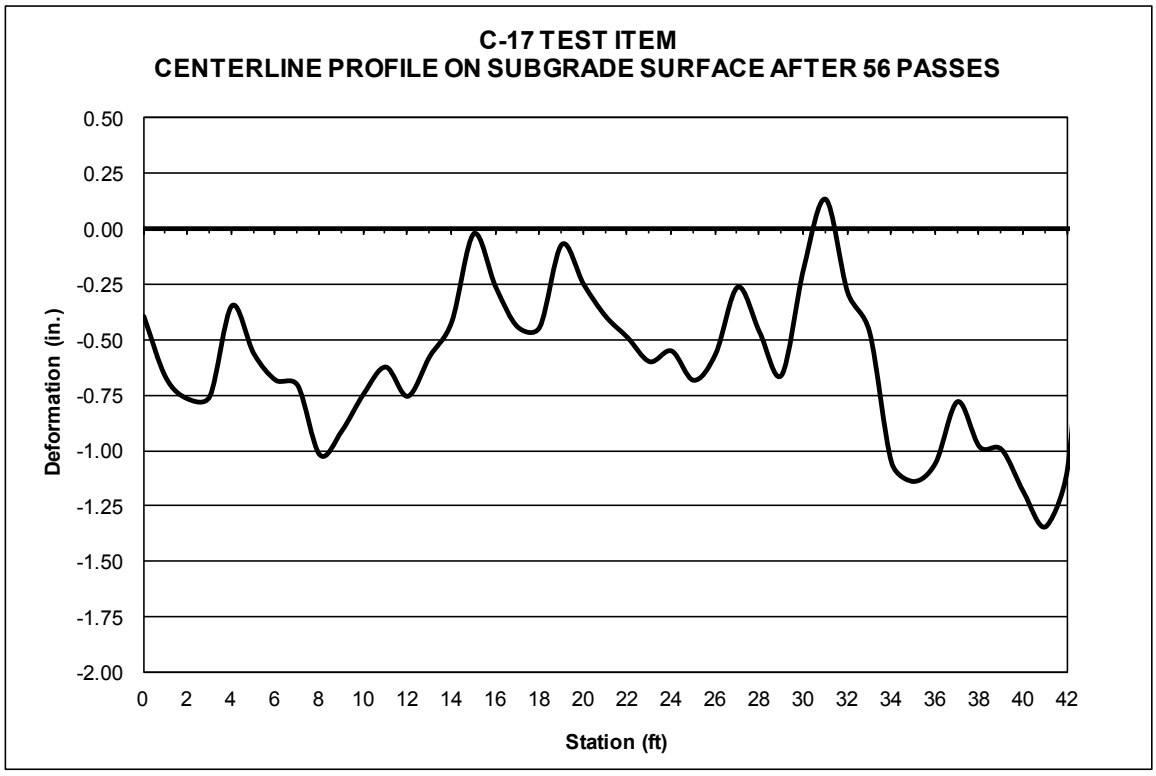

Figure 38. Centerline profile on the mat surface of the F-15E item.

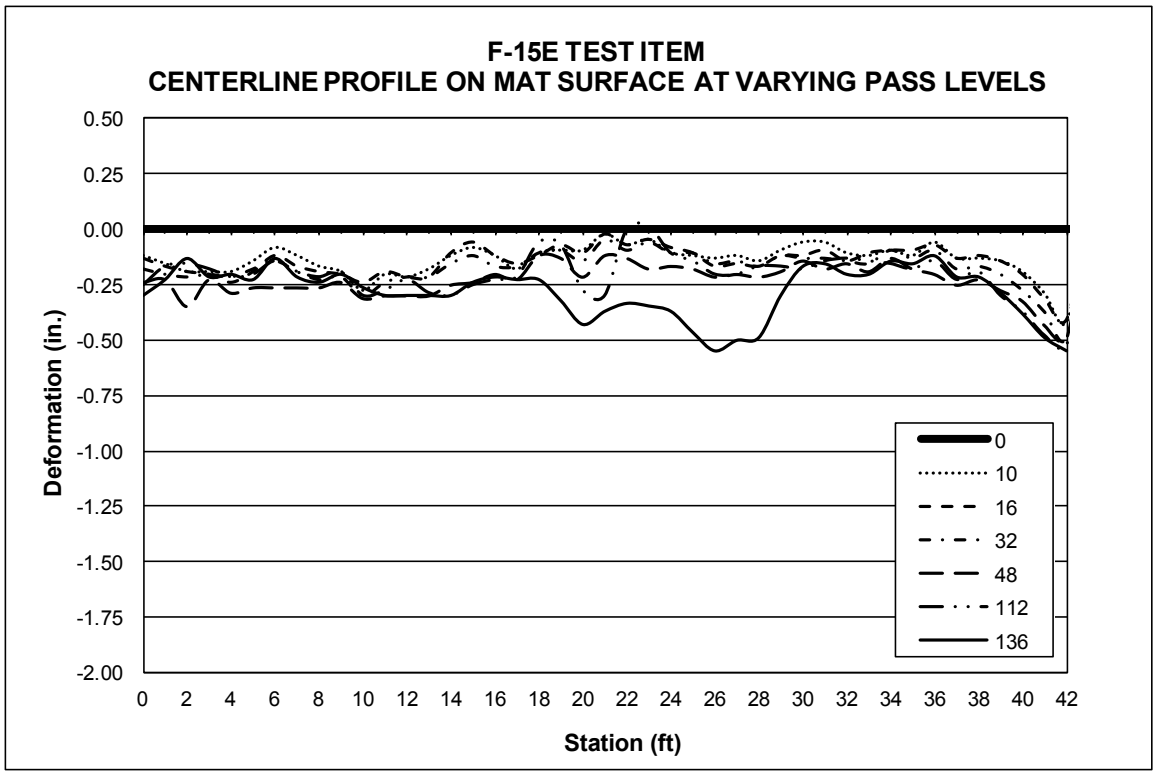

Figure 39. Centerline profile on the mat surface of the C-17 item.

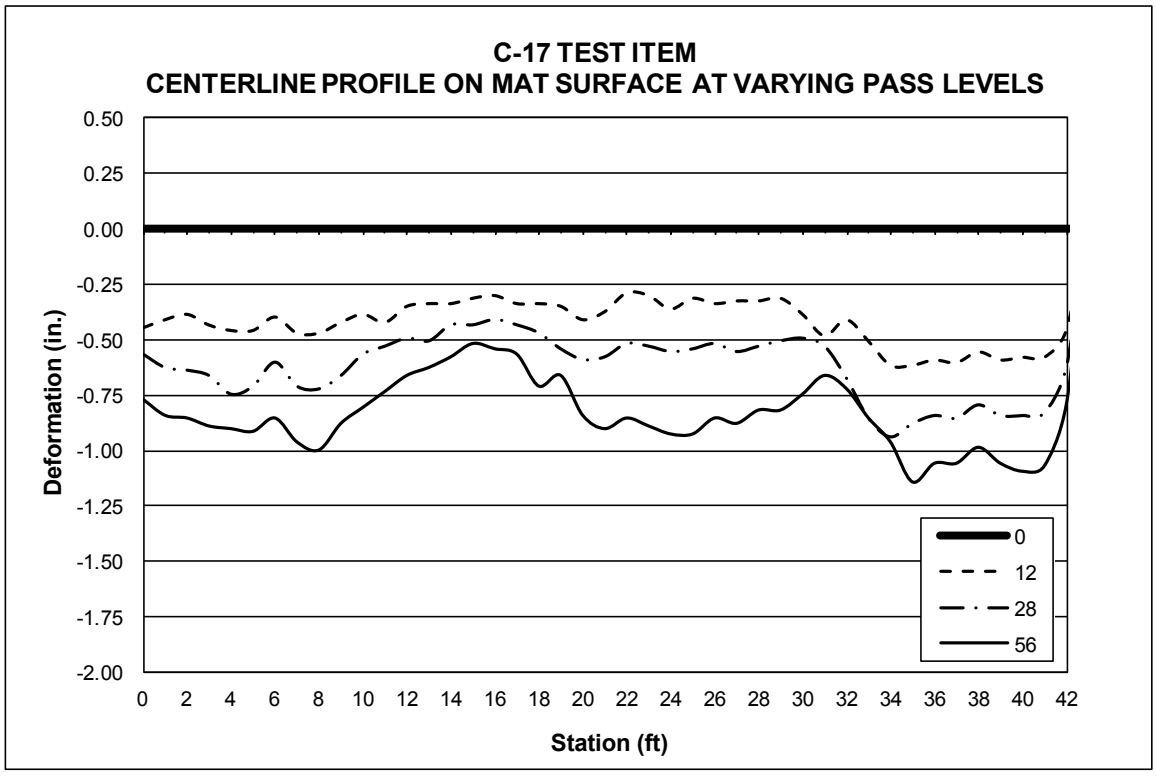

Figure 40. Average deformation on the subgrade of the F-15E item.

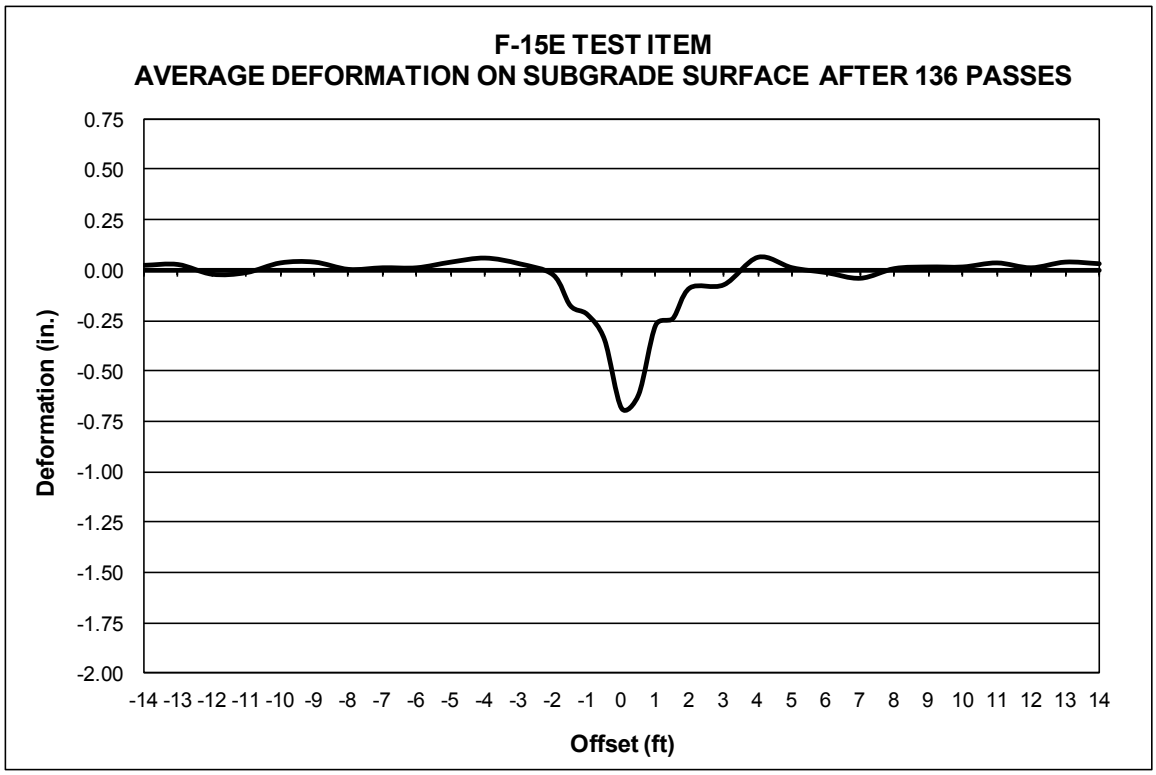

Figure 41. Average deformation on the subgrade of the C-17 item.

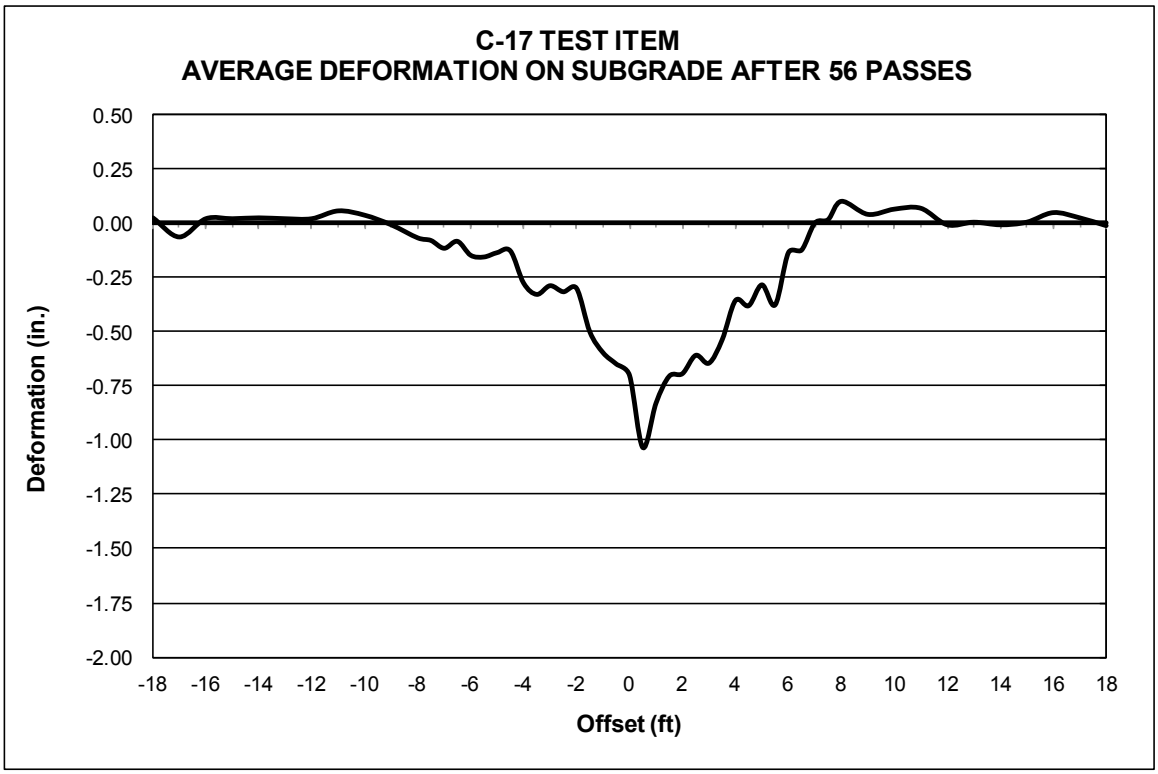

Figure 42. Average deformation on the loaded mat surface of the F-15E item.

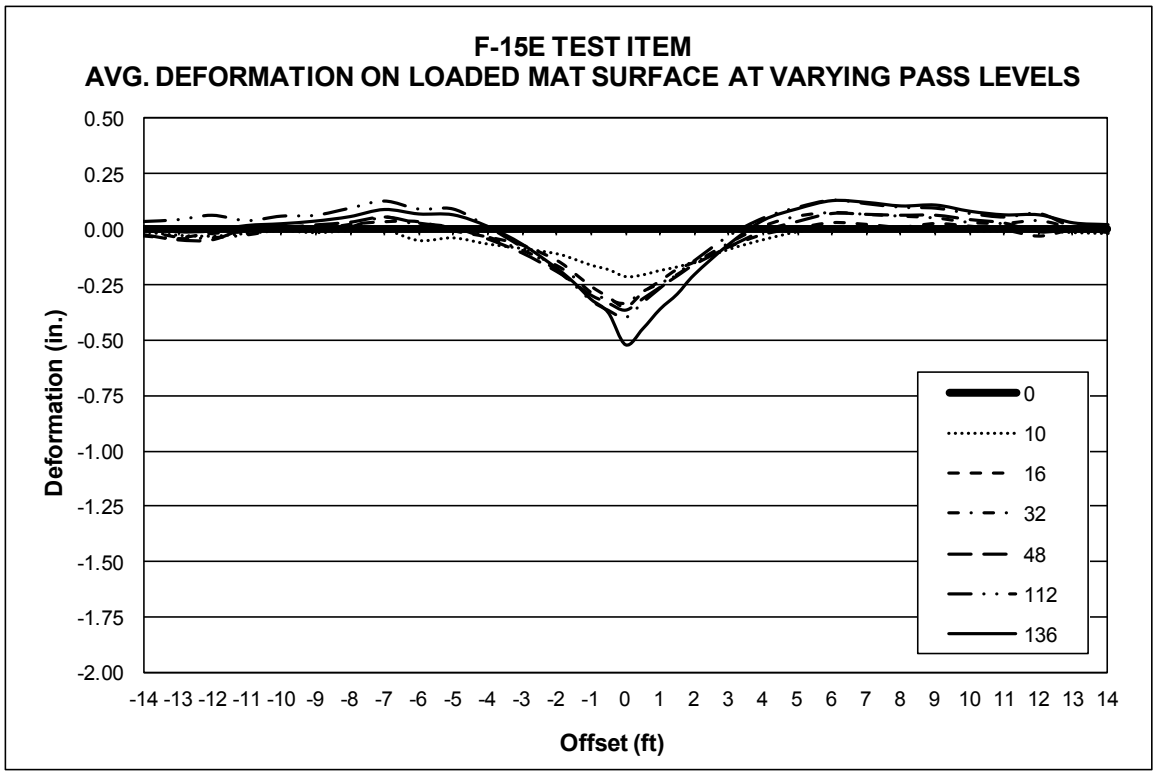

Figure 43. Average deformation on the loaded mat surface of the C-17 item.

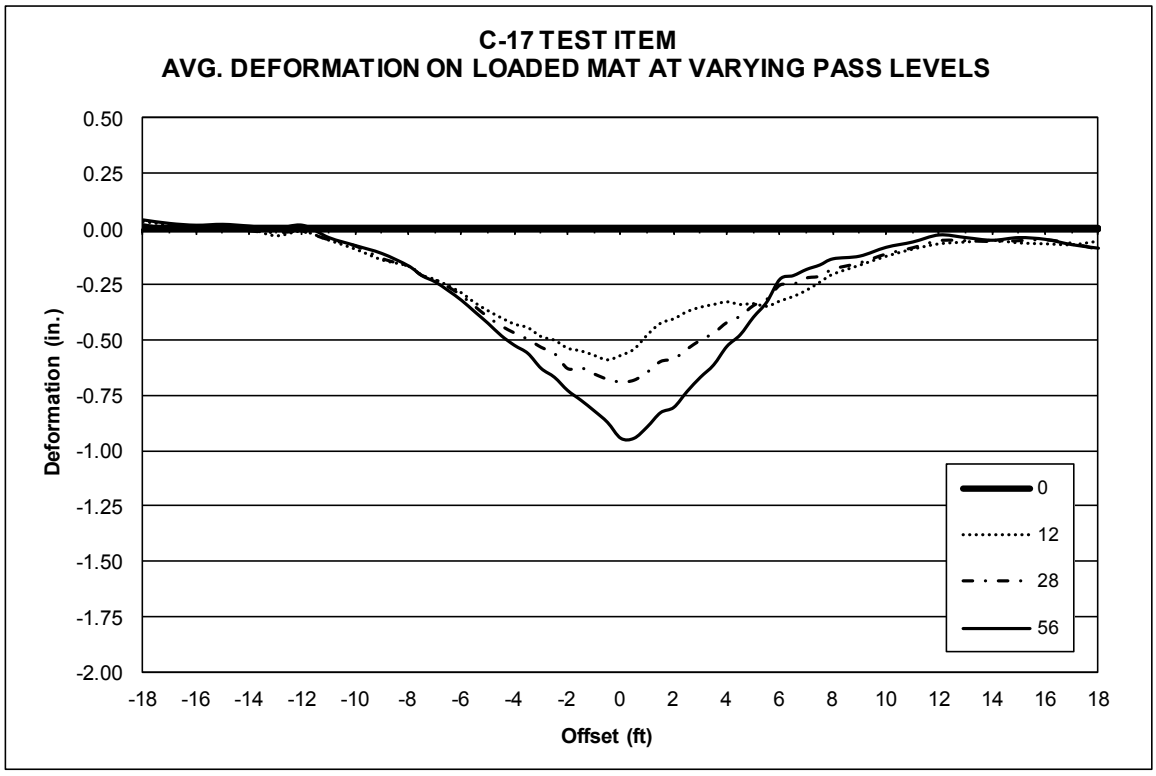

Figure 44. Average deformation on the unloaded mat surface of the F-15E item.

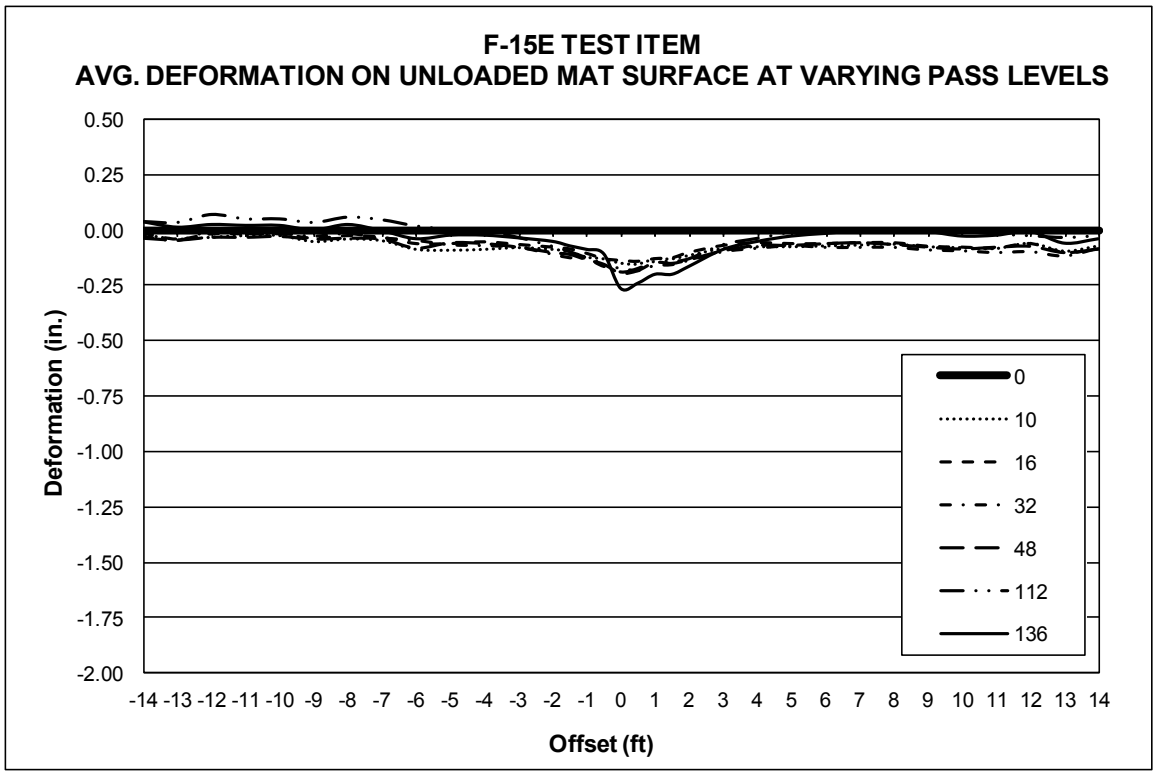

Figure 45. Average deformation on the unloaded mat surface of the C-17 item.

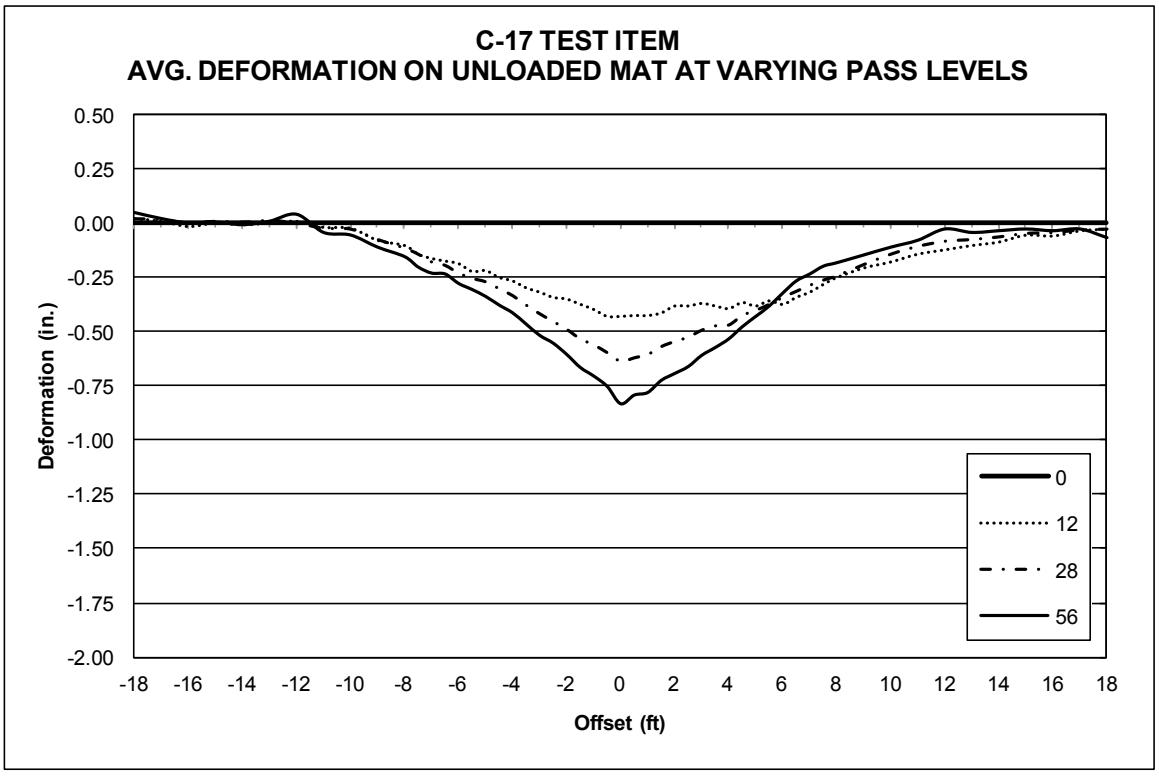

Table 9. Maximum measured permanent deformation values for each test item.

Test Item	Pass Number	Subgrade Profile Max Abrupt Change in Elevation (in.)	Mat Surface Profile Max Abrupt Change in Elevation (in.)	Subgrade Permanent Deformation (in.)	Loaded Deformation on Mat Surface (in.)	Unloaded Deformation on Mat Surface (in.)
F-15E	136	0.90	0.32	0.74	0.62	0.26
C-17	56	0.79	0.48	1.11	0.95	0.85

3.3 Elastic deflection

Elastic deflection was measured on the F-15E item at scheduled pass intervals. Elastic deflection was not measured on the C-17 item because of the inability to mount a survey prism in an acceptable location on the load cart and other safety concerns.

Elastic deflection was determined by mounting a survey prism on the F-15E load cart just above the center of the load wheel. A continuous survey mode was used with the robotic total station so that elevations were recorded each time the load cart moved 6 in. from the previous measurement. Examples of the raw data as collected are shown in Figure 46 and Figure 47. These data were collected dynamically at scheduled pass intervals throughout trafficking. The data were reduced by evaluating the elevation measurements within half a tire width (4.5 in.) from the centerline, as shown as boundaries in Figure 46 and depicted as elevations in Figure 47. Calculations determined the average elevation of points within ± 6 in. of each centerline profile elevation location in terms of northing. The calculated average elevation corresponding to each station was then subtracted from measurements taken on the unloaded mat surface at the same location. For example, the average of dynamic deflections at each station for Passes 1 through 10 was subtracted from the unloaded centerline profile recordings at each station collected at Pass 10. The difference in the loaded and unloaded measurements is the elastic deflection, or rebound, of the mat and subgrade as the test wheel moved over the surface. The average elastic deflection at each station for each data collection interval is shown in Figure 48. For the F-15E item, the elastic deflection stayed approximately 1.2 in. throughout testing. Elastic deflection was not measured at failure (56 passes) to prevent damage to the F-15E tire by tire hazards present in the traffic lane.

Figure 46. Elastic deflection measurements' wander distribution on F-15 item.

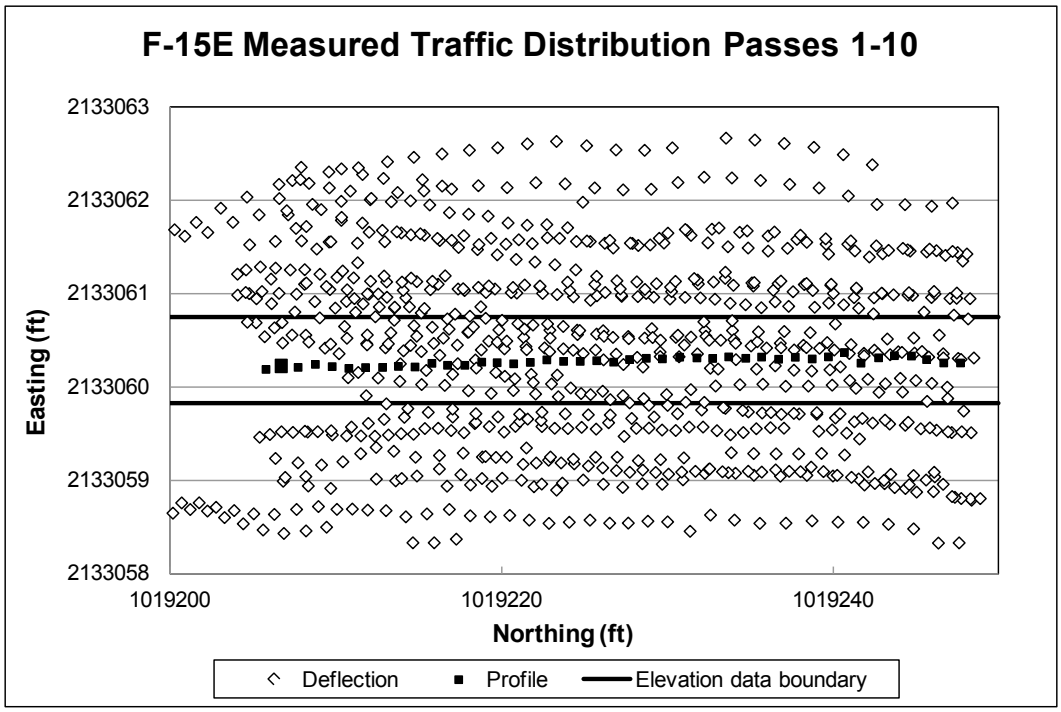

Figure 47. Elastic deflection elevation distribution on F-15 item.

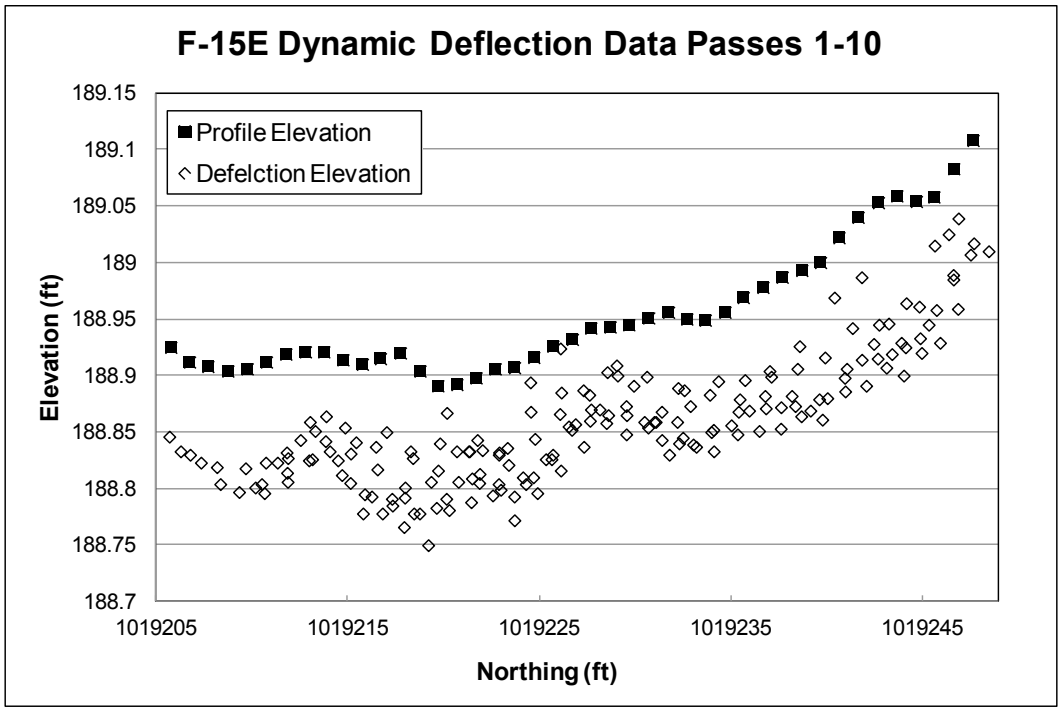

Figure 48. Elastic deflection on F-15 item mat surface at various pass levels.

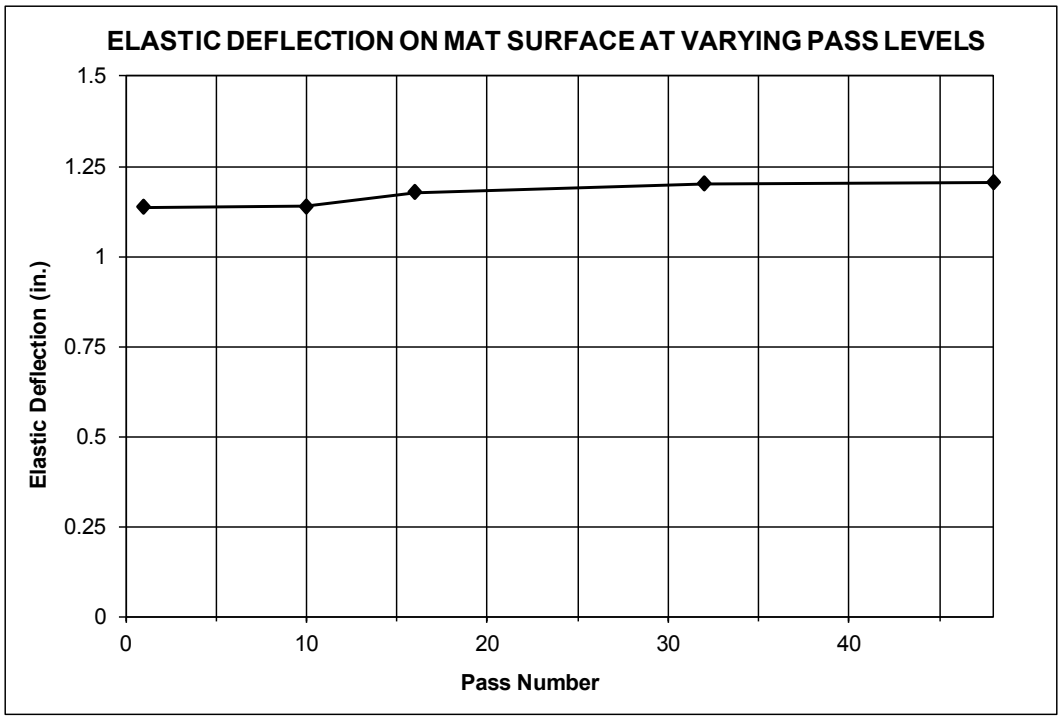

3.4 Strain gauge data

Strain data were recorded at a rate of 100 Hz throughout trafficking for both the F-15E and C-17 test items. Strain gauges were installed as shown in Figure 16 and Figure 18 in regions determined to have the highest stress concentrations and smallest cross-sectional areas. These gauge locations on the upper underlap and lower overlap regions have been shown to be the predominant failure regions in full-scale tests of AM2 reported by Rushing and Tingle (2007), Rushing and Torres (2007), Rushing et al. (2008), Rushing and Mason (2008), and Garcia and Rushing (2013). The data gathered will be used to validate a DIM for NAVAIR and in future modeling efforts by the ERDC.

Example plots of the strain gauge raw data for the F-15E and C-17 items are shown in Figure 49 and Figure 50, respectively. Figure 49 represents the response from the first 10 passes of F-15E traffic from a gauge installed on the upper underlap of Panel 62 (the first panel to fail). Each of the positive peaks represents tensile strains, and the negative peaks represent compressive strains. Each of the 10 passes can be associated with a measured peak. Since the distributed traffic pattern began on the east side of the gauge location, the gauge did not measure significant compressive strains during the first four passes. The data set validates that the load moved to the west

Figure 49. Strain gauge data for F-15E item, SG 62F1, passes 1-10.

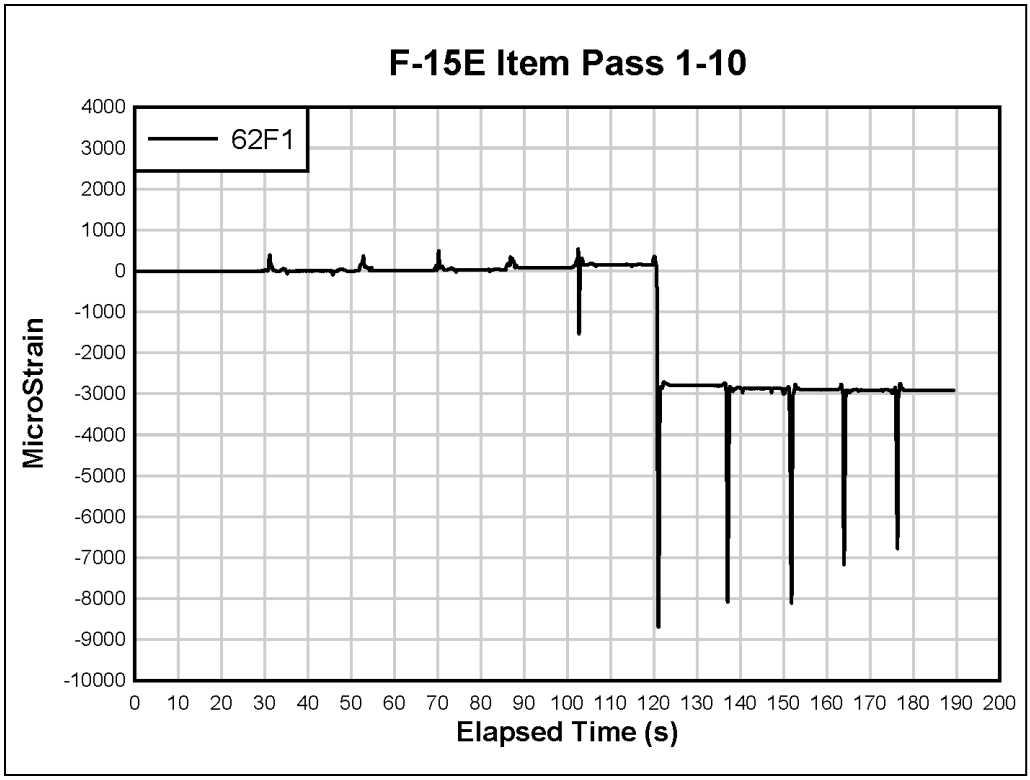

Figure 50. Strain gauge data for C-17 item, SG 61F2, passes 1-12.

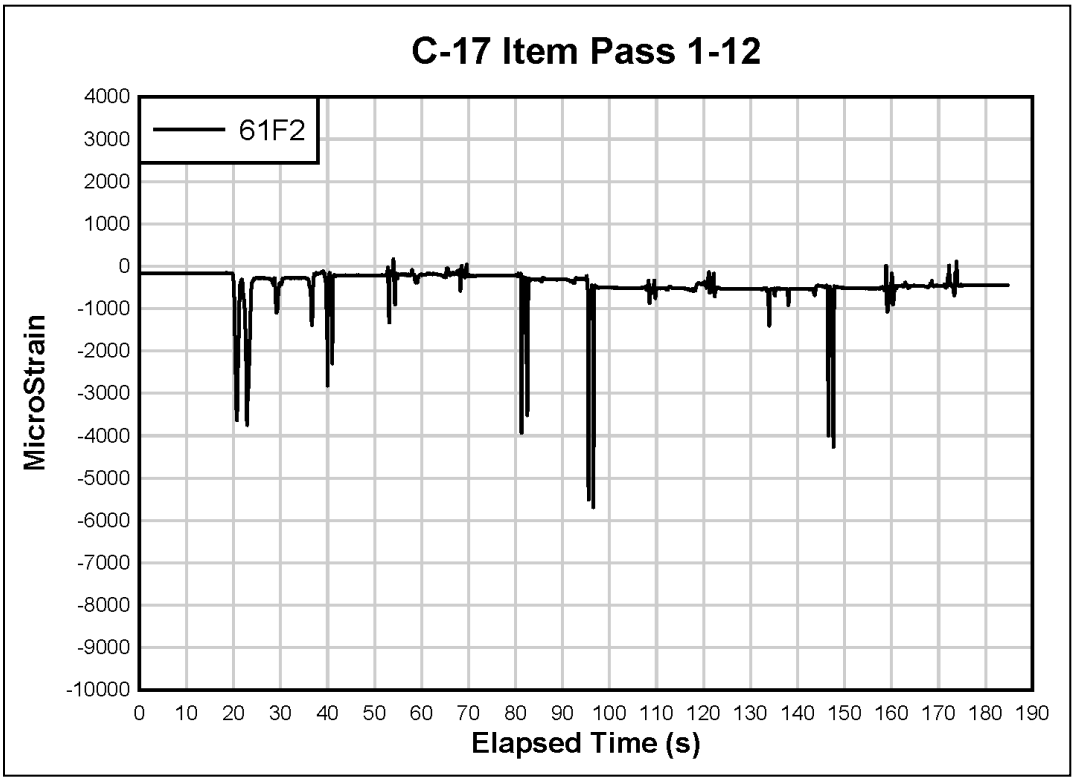

side of the joint on pass six, where there is a baseline shift indicating permanent deformation and large compressive strains. The changing magnitude of the peaks was caused by the wander pattern used to simulate a normal distribution of traffic over the test section. The higher peaks indicate that the load cart was located directly above, or adjacent to, the strain gauge.

Figure 50 represents raw data collected for the first 12 passes of the 6-wheeled C-17 load cart from a strain gauge mounted on the lower overlap of Panel 61 (third panel to fail). Each pass is indicated by two large peaks and one small peak, representing the two main axles of the C-17 and the drive axle of the scraper engine used to pull the simulator, respectively. The strain values generally show higher compressive strains for the first six passes when the vehicle was on the east side of the joint, and then the values tended to decrease when the vehicle moved to the west side of the joint. This reaction is exactly opposite of the effect shown in Figure 49 but is expected, since the opposing panel joints are represented. As described for Figure 49, the magnitudes of the peaks also indicate the wander pattern used in the test, but it is not as obvious, since six load wheels are being applied instead of one.

From the raw data, the maximum tensile strains and the absolute value of the compressive strains were captured for each gauge throughout traffic and are reported in Figure 51 through Figure 62. The values associated with these figures are reported in the Appendix. The full data set is archived at the ERDC and may be made available upon request.

For the F-15E item, Gauge 93F1 failed to function during the test. From Table 7, Panels 62, 69, and 78 failed in the range of 49 to 80 passes as indicated by their disappearance beginning in Figure 55. After the failures, the strains measured on the opposing panels, 63, 70, and 79, were significantly reduced as shown in Figure 56, validating the stress relief in the lower overlap after the upper underlap broke free from the adjacent panel. Other significant inferences from the F-15E data were that the strain magnitude increased, as shown for gauges on Panels 63 and 98, near the bridging panel boundaries from Panels 57 and 104, and strain values increased because of load transfer to successive panel sets after a failure.

For the C-17 item, Figure 60 through Figure 62 show that gauges 76F3, 82F2, and 97F2 failed to return any usable data. According to Figure 61,

data indicate Panels 90 and 97 failed between passes 13 and 28, although visual observations reported failures at 28 and 56 passes, respectively. The strain gauge data may be able to show that failure occurred earlier than noted from visual observations or that high strains may have destroyed the gauges prior to failure. Most likely, the gauge failures are directly linked to mat breakage. The raw strain data validated that Panel 83 failed at 46 passes, and Panels 61, 67, and 76 all failed at 50 passes. The values shown in Figure 62 show the strain magnitudes for these four panels prior to failure. Overall, the measured strains in both test items appeared to yield usable results for the DIM and other future modeling efforts.

Figure 51. Strain gauge data for F-15E item, passes 1-10.

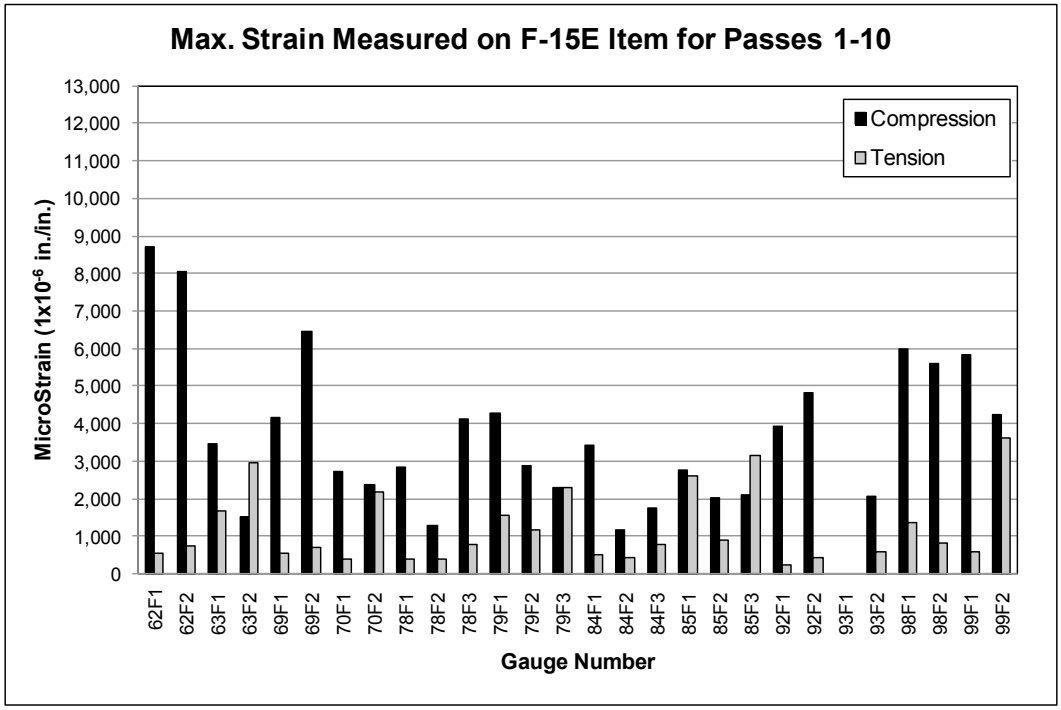

Figure 52. Strain gauge data for F-15E item, passes 11-16.

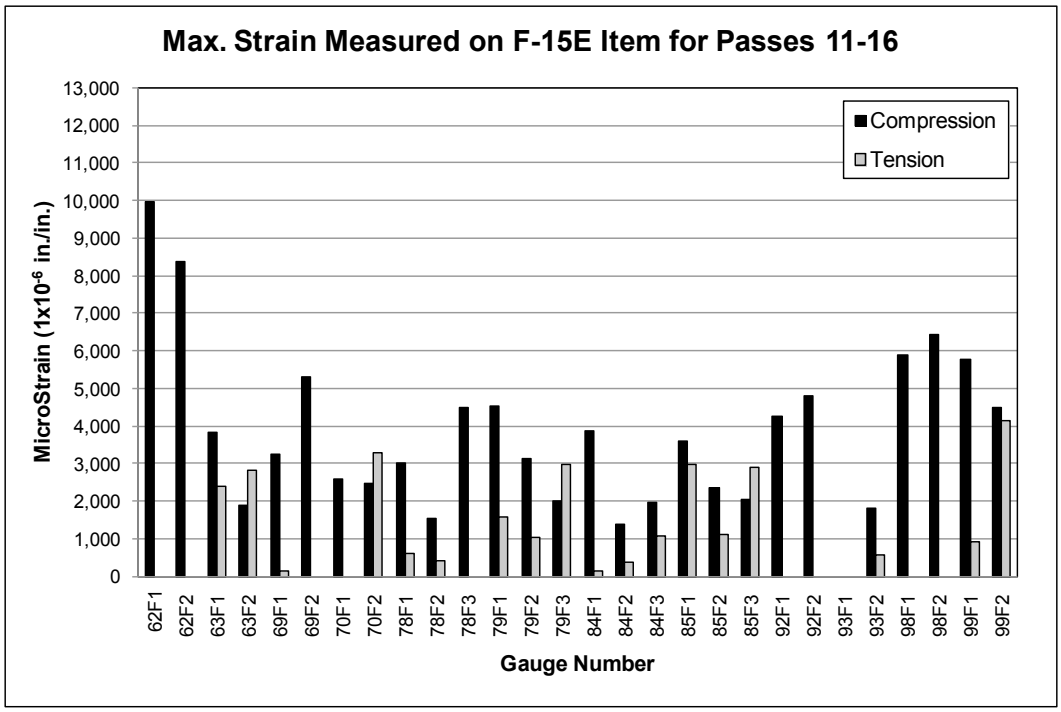

Figure 53. Strain gauge data for F-15E item, passes 17-32.

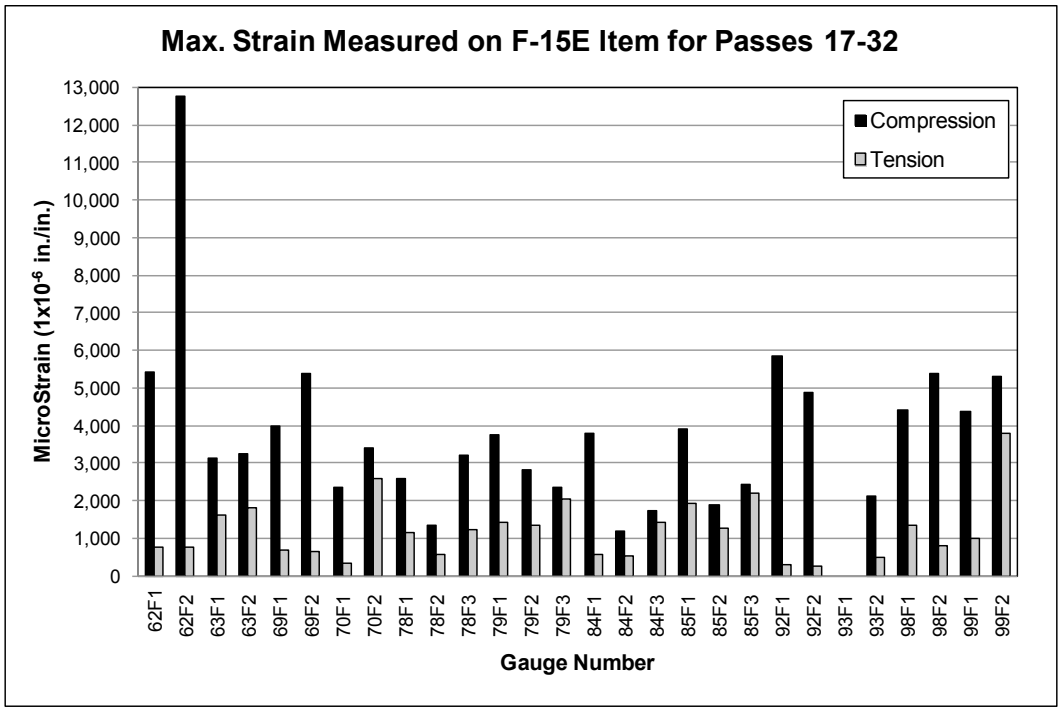

Figure 54. Strain gauge data for F-15E item, passes 33-48.

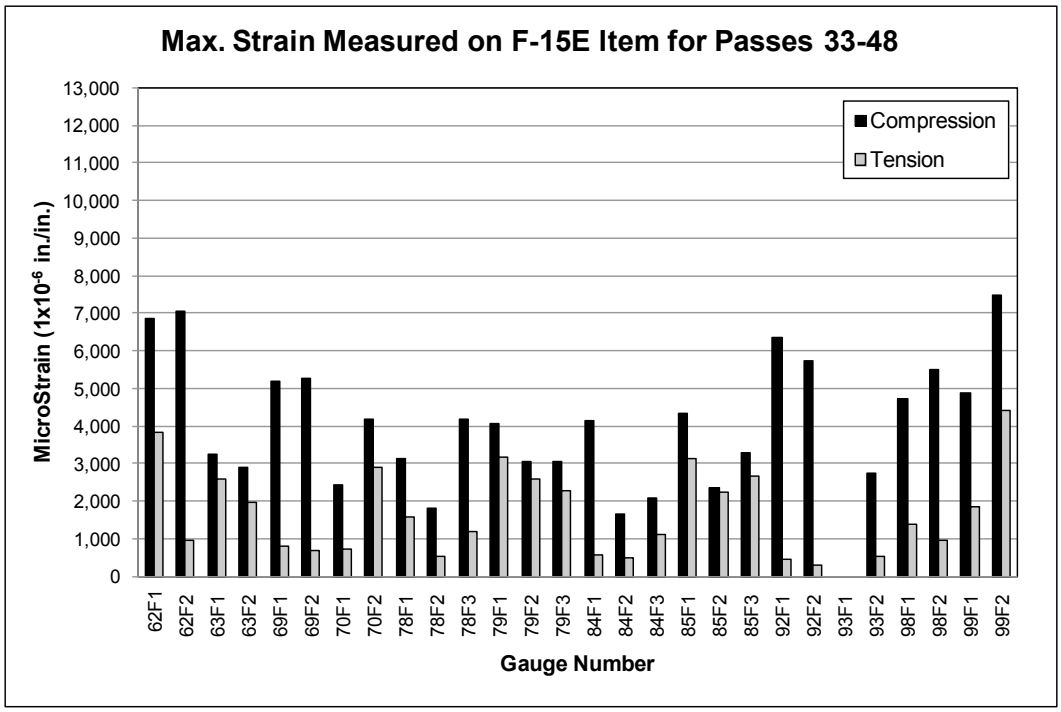

Figure 55. Strain gauge data for F-15E item, passes 49-80.

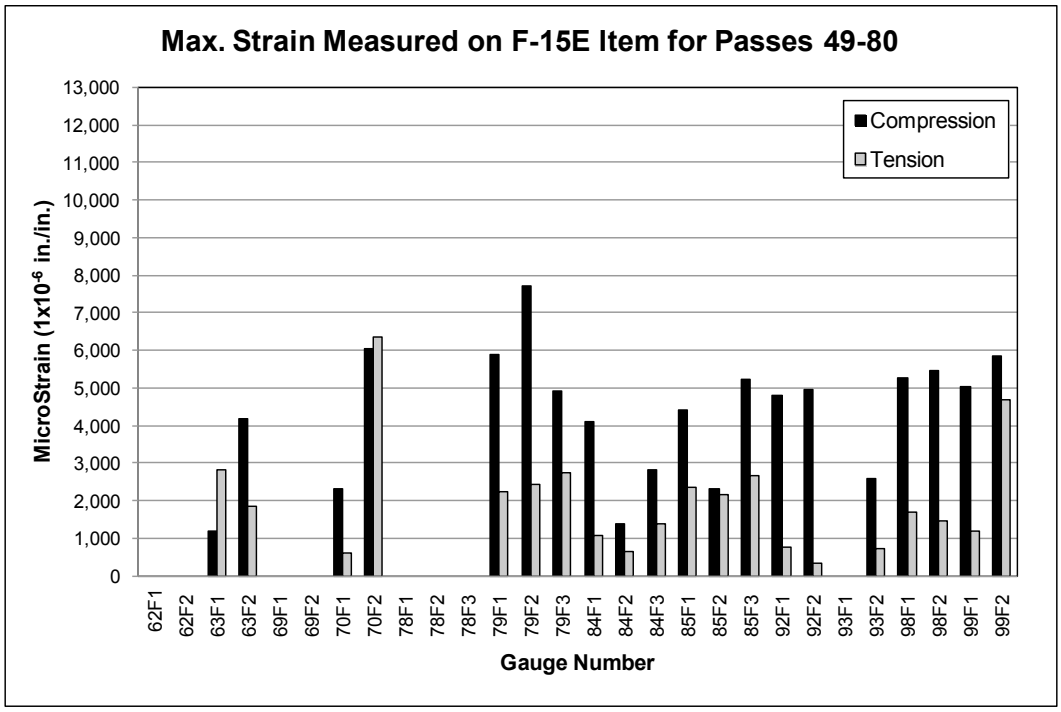

Figure 56. Strain gauge data for F-15E item, passes 81-112.

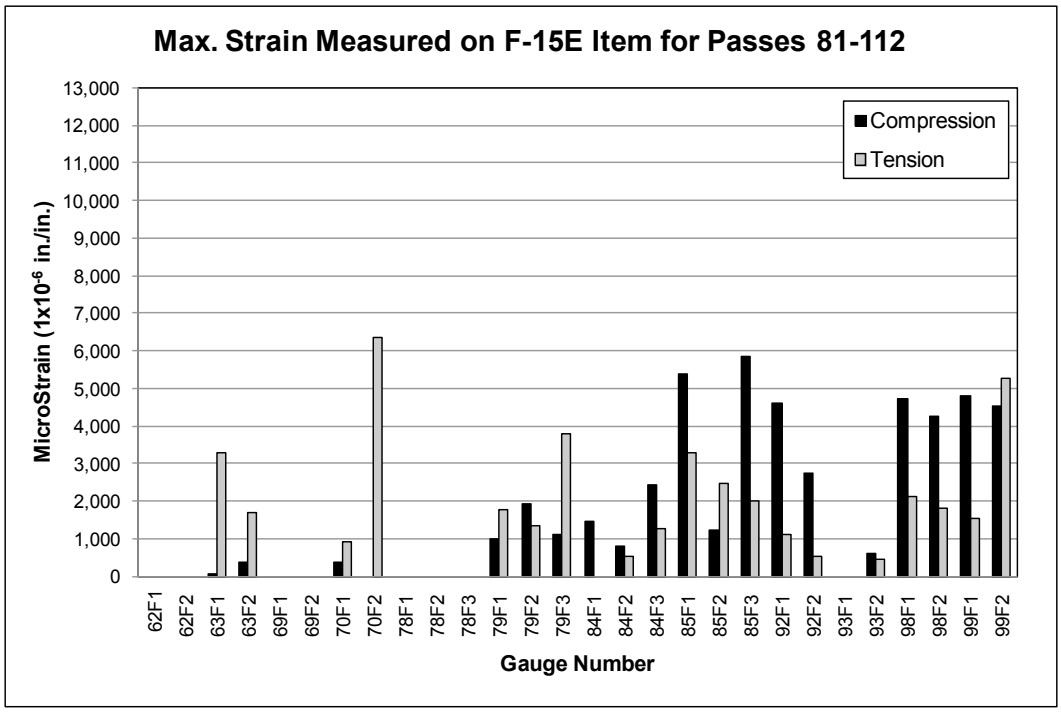

Figure 57. Strain gauge data for F-15E item, passes 113-126.

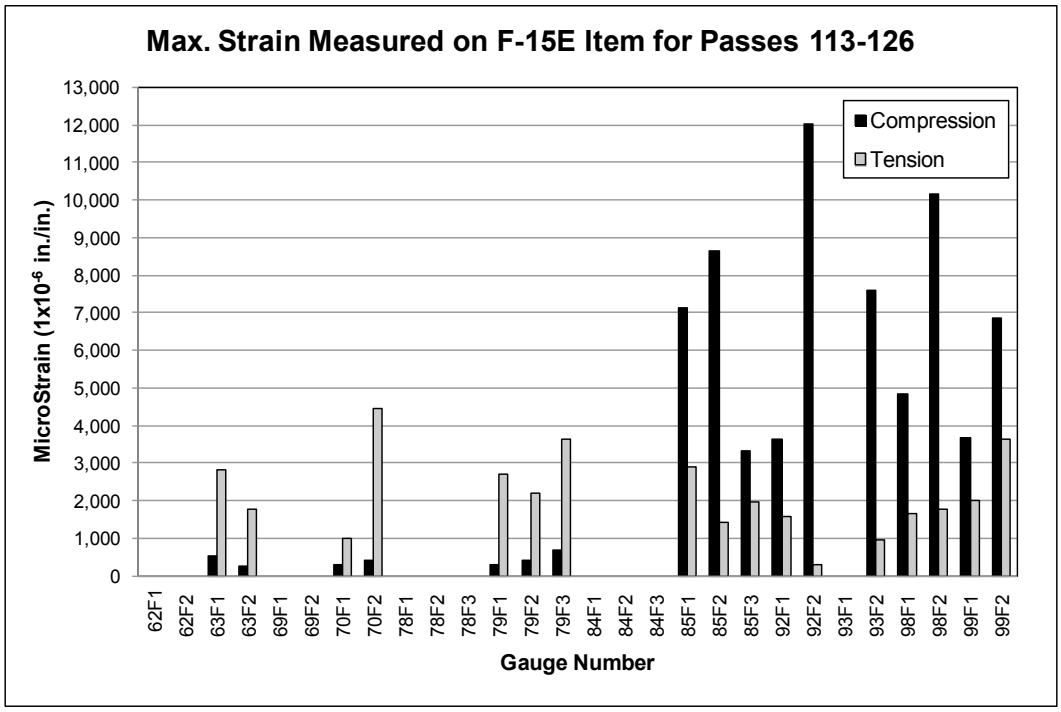

Figure 58. Strain gauge data for F-15E item, passes 127-128.

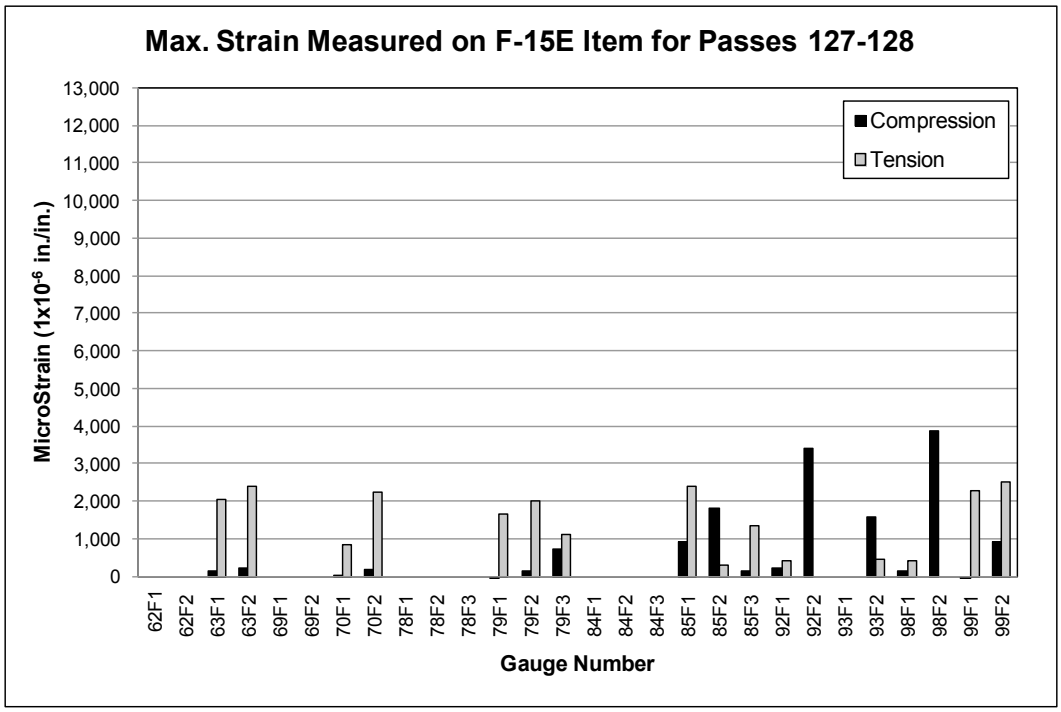

Figure 59. Strain gauge data for F-15E item, passes 129-136.

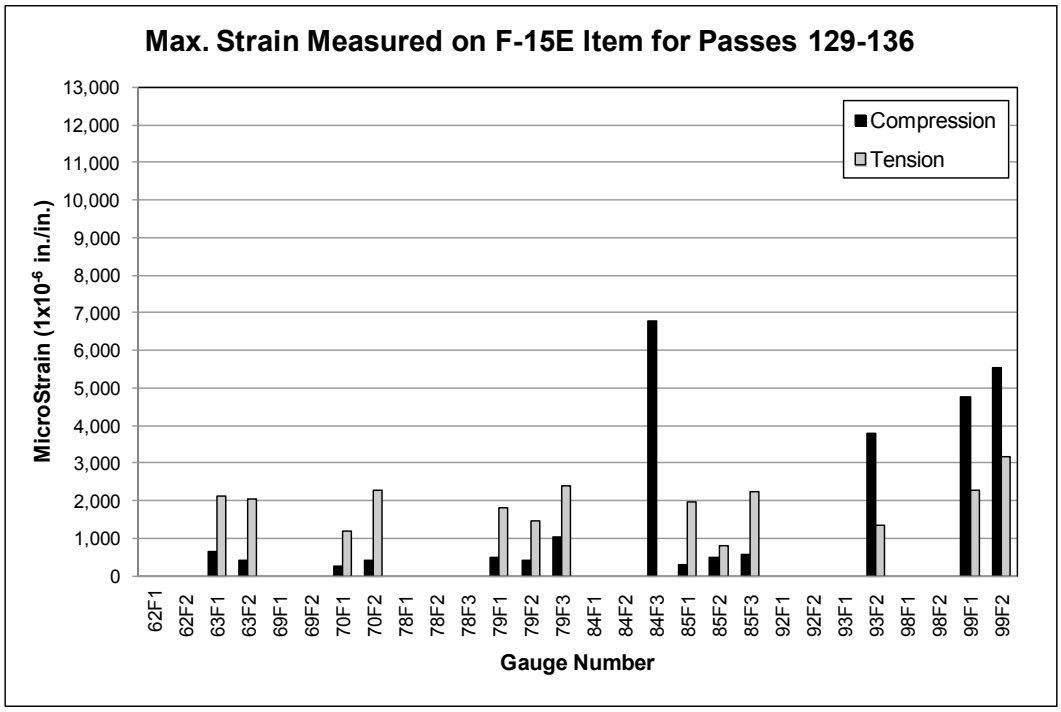

Figure 60. Strain gauge data for C-17 item, passes 1-12.

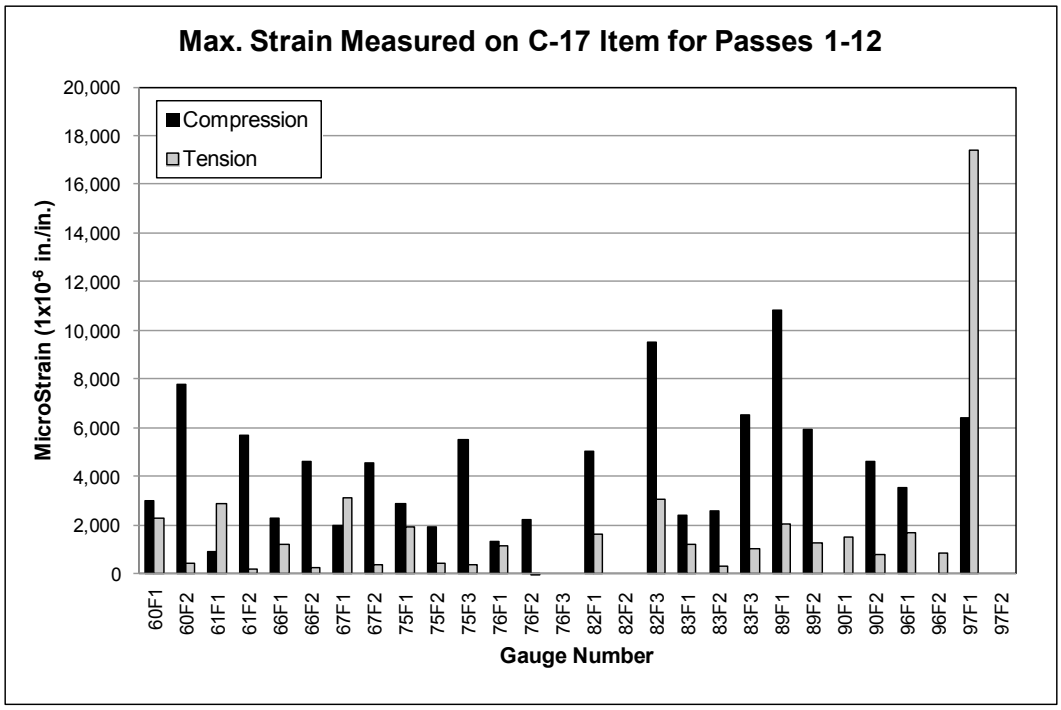

Figure 61. Strain gauge data for C-17 item, passes 13-28.

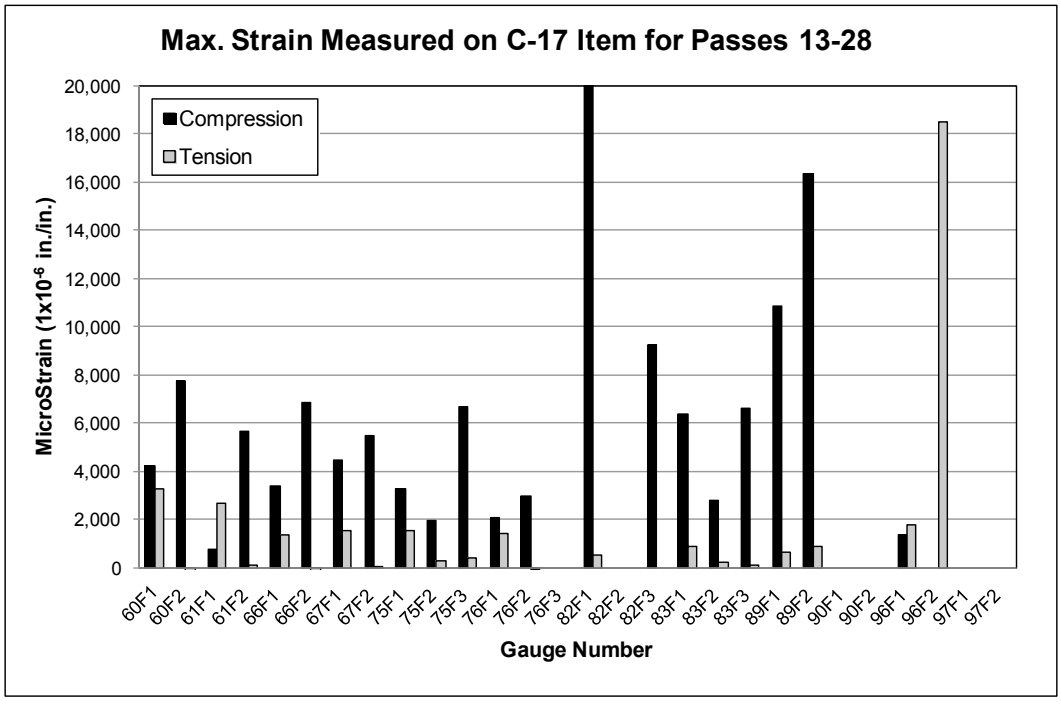

Figure 62. Strain gauge data for C-17 item, passes 29-56.

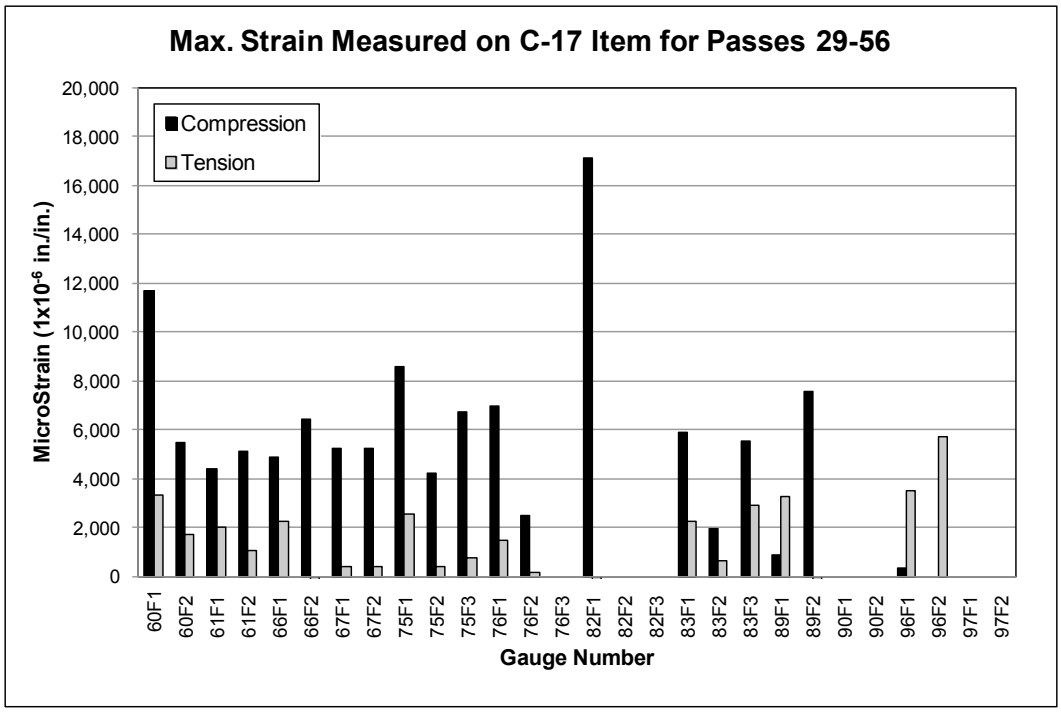

Note: Data reported for Panel 83 are prior to pass 46, and data for Panels 61, 67, and 76 are prior to pass 50 because of panel failures beyond those pass numbers.

4 Analysis of Results

4.1 F-15E test item

4.1.1 Mat breakage

The F-15E test item sustained 135 passes (34 coverages) of simulated F-15E aircraft traffic before failure by mat breakage. Panels failed in succession along the continuous longitudinal joint in the instrumented region of the test array. Failures began in the south with Panel 62 after 62 passes and worked their way north to Panel 98 after 135 passes, as shown in Figure 34. All failures were broken upper underlap rails on the panel's end connectors. This same mode has been documented by Rushing and Tingle (2007), Rushing and Torres (2007), Rushing et al. (2008), Rushing and Mason (2008), and Garcia and Rushing (2013) as the most common form of failure in AM2 Mod 5 when trafficked over weak subgrade conditions. Failures occurred because of stress concentrations in the upper underlap rail located in the corner of the locking bar insertion slot at the interface with the smallest cross sectional area of the rail. Cyclic loading caused a crack to incubate in the described location and then propagate along the end connector until the rail completely separated from the panel causing total failure.

In this test, the 3-4 pattern caused six end joints to be continuous within the test array for a length of 12 ft. This continuous longitudinal joint arrangement greatly decreased the number of passes to failure. The AM2 standard brickwork pattern, evaluated by Rushing and Tingle (2007) and Rushing and Torres (2007), under F-15E traffic over a subgrade of similar strength failed after about 1,500 passes, but had an unsupported length of only one panel, or 2 ft. The continuous end connector joint allowed the panels to rotate downward until the upper underlap rail was fully engaged with the opposing upper overlap. Large strains occurred in the upper underlap as soon as the traffic loading was applied to the west side of the end joint. The 3-4 pattern also increased the rate of permanent deformation in the subgrade, which further accelerated failure by allowing larger strains to be induced in the joints early in the trafficking sequence.

Interestingly, all of the panel damage occurred on strain gauge instrumented panels. To facilitate strain gauge installation, material was removed from the opposite joint in the area it would normally contact the gauge location. Finite element models of the joint predicted that changes in applied stress and resulting strains would not occur from removing this small section of the mat joints (about 1 in. per gauge). While researchers agree that the strain gauge installation procedures should not have significantly reduced performance, it is possible that there was an unintended effect on behavior that caused accelerated failure.

In terms of mat breakage, a reduction in performance of about 90 % occurred in the 3-4 pattern in relation to the number of passes to mat breakage failure reported for the brickwork configuration. As the strength of the subgrade is increased, this reduction factor is expected to decrease. Testing of AM2 over a CBR of 25 by Garcia et al. (2014), showed that the mode of failure of AM2 tends to shift from the joint to the panel's interior around a CBR of 25. This shift in the failure location for the brickwork configuration occurred, because the subgrade was strong enough to carry the applied load with minimal permanent deformation. Since the mat did not rotate enough to engage the upper underlap or lower overlap rails, rail failures were slow to occur. Failures were shifted into the interior vertical stiffeners that comprised the panel's core and were caused by buckling under repeated loadings. When testing AM2 under F-15E traffic over a CBR of 25, mat breakage failure occurred after about 6,300 passes.

4.1.2 Permanent deformation

4.1.2.1 Centerline profile

The centerline profiles for the post-traffic subgrade and the surface of the mat at various traffic intervals are shown in Figure 36 and Figure 38, and maximum values are reported in Table 9. Both profiles were analyzed to determine whether the roughness criterion was exceeded. The values in Table 9 are 0.90 in. and 0.32 in. for the subgrade and mat surface, respectively, and are below the 1.25-in.-deep maximum value established for roughness for F-15E aircraft traffic. Therefore, the system performed adequately to prevent excessive roughness from occurring along the profile during the application of 136 passes. Similar behavior was also documented in previous brickwork pattern tests over a CBR of 6 (Rushing and Tingle 2007; Rushing and Torres 2007).

4.1.2.2 Cross sections

The permanent deformation on the subgrade, the loaded mat surface, and the unloaded mat surface is shown in Figure 40, Figure 42, and Figure 44, respectively. For the F-15E test item, the maximum permanent deformation after 135 passes was 0.74 in., 0.62 in., and 0.26 in. on the subgrade, loaded, and unloaded mat surface, respectively. The failure criterion of 1.25 in. was not exceeded. Therefore, the system performed adequately to prevent excessive roughness from occurring prior to failure by mat breakage. In previous tests over a CBR of 6 using the brickwork pattern, deformation limits were exceeded around 1,500 passes.

4.1.3 Elastic deflection

The elastic deflection measurements shown in Figure 48 were the sum of the gap between the bottom surface of the mat and the top surface of the subgrade when the mat was unloaded (elastic deflection of the mat) and the elastic deflection of the subgrade. The elastic deflection generally remained constant throughout the traffic test at approximately 1.20 in. Previous tests demonstrated an increase in elastic deflection as the test progressed; however, since trafficking was stopped after only 136 passes, the limited number of data ranges evaluated may not have been sufficient for a similar trend to develop. The constant measurement seems to indicate that the distance between the mat and the subgrade stayed relatively constant and that the mat surface moved downward with the permanent deformation in the subgrade. This is reasonable, since the increased number of joints along the wheel path for the 3-4 pattern when compared to the brickwork pattern increases the flexibility and reduces the global stiffness of the test array.

4.1.4 Strain gauge readings

Strain gauges were installed on the upper underlap and lower overlap end connector rails to determine strain magnitudes under simulated aircraft traffic for validation of a DIM for NAVAIR and for future modeling efforts at the ERDC. Analysis of the data from this test showed that the gauges performed as designed, and the measured strains appeared to be reasonable. Compressive strains were much greater than tensile strains and controlled the failure of the rails under cyclic loading. The gauge data were able to validate the pass numbers at which individual gauged mat panels failed by counting the pass where the data became unusable. The data indicated that strains were elevated near the interface of changing boundary

conditions where the ability of the mat system to move downward was limited. The data also proved that as one panel failed, the strains in the matting panel on the opposite side of the joint were significantly reduced. The data showed that once a joint failed, the load was transferred to the adjacent joint and the strains increased. This behavior validates the progressive failure observed in the test where the six in-line joints appeared to un-zip as traffic was continued. Prior to panel failures, typical compressive strains varied from 1,000 to 10,000 microstrain.

Identical tests are planned with panels arranged in the brickwork and 2-1 pattern for a direct comparison of strains and number of passes to failure. Once all data have been collected, an in-depth analysis of the strain behavior for the three patterns will be conducted to further improve understanding of the fatigue behavior or the AM2 joint system.

4.2 C-17 test item

4.2.1 Mat breakage

The C-17 test item was trafficked until 56 passes (50 coverages) were completed and six panels (8%) had failed by mat breakage. Traffic was stopped because of the imminent threat to the tires of the traffic simulator. All panel failures were in the instrumented region of the test array beginning with Panel 90 after 28 passes, then Panel 83 after 46 passes, Panels 61, 67, and 76 after 50 passes, and finally Panel 97 after 56 passes, as shown in Figure 34. All failures were broken lower overlap rails on the panels' end connectors.

Similar modes of failure have been documented in previous tests of AM2 Mod 5; however, the majority of failures have historically been upper underlap rail failures with only a few lower overlap failures. The cause of the change in the predominant mode of failure is unknown. However, it may be linked to one of two changes from previous tests: (1) six continuous end connector joints increased the ability of the joints to rotate and (2) 6-ft panels were installed along the centerline, as shown in Figure 34, which likely further increased the rotational freedom along the joints. Similarly as described for the F-15E, the end connector failures occurred because of stress concentrations in the lower overlap rail located in the corner of the locking bar insertion slot at the interface with the smallest cross sectional area of the rail. Cyclic loading caused a crack to incubate in the area of high-stress concentration and then propagate along the end connector until the rail completely separated from the panel, causing failure.

In this test, the 3-4 pattern caused six end joints to be continuous within the test array for a length of 12 ft, greatly decreasing the number of passes to failure. The AM2 standard brickwork pattern evaluated by Rushing and Tingle (2007) under C-17 traffic over a subgrade of similar strength failed after about 1,500 passes but had an unsupported length of only one panel, or 2 ft. The long end connector joint allowed the panels to rotate downward until the lower overlap rail was fully engaged with the opposing lower underlap. Large strains occurred in the lower overlap as soon as the traffic loading was applied to the east side of the end joint. The 3-4 pattern also increased the rate of permanent deformation in the subgrade, which further accelerated failure by allowing larger strains to be induced in the joints early in the trafficking sequence.

As noted for the F-15E test item, all of the panel damage occurred on strain gauge instrumented panels. To facilitate strain gauge installation, material was removed from the opposite joint in the area where it would normally contact the gauge location. Finite element models of the joint predicted that changes in applied stress and resulting strains would not occur from removing this small section of the mat joints for each gauge (about 1 in. per gauge). While researchers agree that the strain gauge installation procedures should not have significantly reduced performance, it is possible that there was an unintended effect on behavior that caused accelerated failure.

In terms of mat breakage, a reduction in performance of about 96 % occurred in the 3-4 pattern in relation to the number of passes to mat breakage failure reported for the brickwork configuration over a similar strength subgrade. As the strength of the subgrade is increased, this reduction factor is expected to decrease along with permanent deformation of the subgrade. Recent testing of AM2 over a CBR of 25 by Garcia et al. (2014), showed that the mode of failure of AM2 tends to shift from the joint to the interior of the panel around a CBR of 25. This shift in the failure location for the brickwork configuration occurred because the subgrade was strong enough to carry the applied load with minimal permanent deformation. Since the mat did not rotate enough to engage the upper underlap or lower overlap rails until late in the test, rail failures were slow to occur. Some failures were shifted into the interior vertical stiffeners that comprised the panel's core and were caused by buckling under repeated loadings. When testing C-17 traffic over a CBR of 25, no mat breakage failures had occurred when traffic was stopped after about 10,000 passes.

4.2.2 Permanent deformation

4.2.2.1 Centerline profile

The centerline profiles for the post-traffic subgrade and the surface of the mat at various traffic intervals are shown in Figure 37 and Figure 39, and maximum values are reported in Table 9. Both profiles were analyzed to determine whether the roughness criterion was exceeded. The values in Table 9 are 0.79 in. and 0.48 in. for the subgrade and mat surface, respectively, and are below the 3.0-in.-deep maximum value established for roughness for C-17 aircraft traffic. Therefore, the system performed adequately to prevent excessive roughness from occurring along the profile after 56 passes. Similar behavior was also documented in previous brickwork pattern tests over a CBR of 6 (Rushing and Tingle 2007).

4.2.2.2 Cross sections

The permanent deformation on the subgrade, the loaded mat surface, and the unloaded mat surface is shown in Figure 41, Figure 43, and Figure 45, respectively. For the C-17 test item, the maximum permanent deformation after 56 passes was 1.11 in., 0.95 in., and 0.85 in. on the subgrade, loaded, and unloaded mat surface, respectively. The failure criterion of 3.0 in. was not exceeded. Therefore, the system performed adequately to prevent excessive roughness from occurring prior to failure by mat breakage. In previous tests over a CBR of 6 using the brickwork pattern, deformation limits were exceeded around 1,500 passes.

4.2.3 Strain gauge readings

Strain gauges were installed on the upper underlap and lower overlap end connector rails to determine strain magnitudes under simulated aircraft traffic for validation of a DIM for NAVAIR and future modeling efforts at the ERDC. Analysis of the data from this test showed that the gauges performed as designed, and the measured strains appeared to be reasonable. Compressive strains were much greater than tensile strains (except for Panel 97) and controlled the failure of the rails under cyclic loading. The gauge data were able to validate the pass numbers at which individual, gauged mat panels failed by counting the pass where the data became unusable. The data indicated that strains were elevated near the interface of changing boundary conditions where the ability of the mat system to move downward was limited. The data showed that strains in the

upper underlap rail were typically greater than those in the lower overlap, although the lower overlap failed in every case.

The data also proved that as one panel failed, the strains in the matting panel on the opposite side of the joint were significantly reduced. Overall, the strains continually increased during the test, and significant increases were noted just prior to panel failure. During the first 12 passes, typical compressive strains varied from 1,000 to 10,000 microstrain. Identical tests are planned with panels arranged in the brickwork and 2-1 pattern for a direct comparison of strains and number of passes to failure. Once all data have been collected, an in-depth analysis on the strain behavior for the three patterns will be conducted to further improve understanding of the fatigue behavior or the AM2 joint system.

5 Conclusions and Recommendations

5.1 Conclusions

The objectives of the effort described herein were to evaluate the NAVAIR AM2 3-4 lay pattern under simulated F-15E and C-17 aircraft traffic over a subgrade with a CBR of 6 to determine the number of allowable passes and to record strain and subgrade deformation data to calibrate the NAVAIR DIM. Permanent deformation and mat breakage were monitored to determine the number of passes to predetermined failure criteria. The results from the test section were compared to those documented in previous tests where AM2 was installed in a brickwork configuration and tested under identical loading and subgrade support conditions. The information obtained from this evaluation will be used to determine operational limitations when AM2 is installed in a 3-4 pattern.

The following conclusions were derived from accelerated traffic testing of the AM2 airfield matting system conducted in May 2013:

- The AM2 F-15E test item assembled in the NAVAIR 3-4 pattern sustained 135 passes (34 coverages) of simulated F-15E aircraft operations on a CH subgrade with a CBR of 6 before failure by mat breakage.
- The number of allowable F-15E operations on AM2 placed over a CBR of 6 was reduced by approximately 90% (from 1,500 to 135) when assembled in the 3-4 pattern instead of a brickwork pattern.
- The AM2 C-17 test item assembled in the NAVAIR 3-4 pattern sustained 56 passes (50 coverages) of simulated C-17 aircraft operations on a CH subgrade with a CBR of 6 before six panel failures occurred (8% mat breakage).
- The number of allowable C-17 operations on AM2 placed over a CBR of 6 was reduced by approximately 95% (from 1,500 to 56) when assembled in the 3-4 pattern instead of a brickwork pattern.
- All mat breaks were caused by failure of upper underlap or lower overlap end connector rails. These failure types are common for the brickwork configuration, but their rate of failure was greatly accelerated by increasing the length of unsupported end connections from a single panel to six panels.

- The strain gauges placed on areas of high-stress concentrations of the upper underlap and lower overlap end connector rails functioned as designed to monitor strains during trafficking. Initial data analysis showed that the gauge responses correctly followed the expected load paths. Compressive strains during the first few passes of both the F-15E and C-17 ranged from 1,000 to 10,000 microstrain, depending on installation location and position of the aircraft simulator. Strain values will be compared to results from identical traffic tests of AM2 assembled in the brickwork and 2-1 patterns for comparison and inclusion in the NAVAIR DIM.

5.2 Recommendations

Based on the airfield mat evaluations described herein, the following recommendations are provided:

- The results of the test described herein validated that the AM2 3-4 pattern is not recommended for use on runways as described in NAWCADLKE-MISC-48J200-0011.
- The AM2 3-4 pattern is recommended only for a subgrade with a CBR ≥ 25 to prevent excessive maintenance and panel replacement requirements.
- When using the 3-4 pattern, the airfield should be designed to minimize the number of continuous end connector joints in the primary wheel paths of the most common aircraft using the facility.

References

ASTM International. 2008. *Standard test method for determination of water (moisture) content of soil by microwave oven heating*. Designation: D 4643-08. West Conshohocken, PA.

ASTM International. 2010. *Standard test method for in-place density and water content of soil and soil-aggregate by nuclear methods (shallow depth)*. Designation: D 6938-10. West Conshohocken, PA.

Garcia, L. T., T. W. Rushing, B. A. Williams, and C. A. Rutland. *AM2 100 CBR subgrade sensitivity test*. ERDC/GSL TR (in preparation). Vicksburg, MS: U.S. Army Engineer Research and Development Center.

Garcia, L., T. W. Rushing, and Q. S. Mason. 2014. *AM2 25 CBR subgrade sensitivity test*. ERDC TR-14-7. Vicksburg, MS: U.S. Army Engineer Research and Development Center.

Garcia, L. T. and T. W. Rushing. 2013. *AM2 sand subgrade sensitivity test*. ERDC/GSL TR-13-10. Vicksburg, MS: U.S. Army Engineer Research and Development Center.

Garcia, L., T. W. Rushing, and Q. S. Mason. 2012. *Evaluation of Webcore prototype AMX mat system*. ERDC/GSL TR-12-14. Vicksburg, MS: U.S. Army Engineer Research and Development Center.

NAWCADLKE. 2006. *Expeditionary airfield AM2 mat certification requirements*. NAWCADLKE-MISC-48J200-0011. Lakehurst, NJ: Naval Air Warfare Center, Aircraft Division.

Rushing, T. W., L. Garcia, and Q. S. Mason. 2012. *Evaluation of Faun aluminum mat systems*. ERDC/GSL TR-12-32, Vicksburg, MS: U.S. Army Engineer Research and Development Center.

Rushing, T. W., L. Garcia, and Q. S. Mason. 2011. *Large-scale 6-CBR prototype mat system evaluation for the AMX program*. ERDC/GSL TR-11-37. Vicksburg, MS: U.S. Army Engineer Research and Development Center.

Rushing, T. W., and J. S. Tingle. 2007. *AM2 and M19 airfield mat evaluation for the rapid parking ramp expansion program*. ERDC/GSL TR-07-5. Vicksburg, MS: U.S. Army Engineer Research and Development Center.

Rushing, T. W., and N. Torres. 2007. *Prototype mat system evaluation*. ERDC/GSL TR-07-29. Vicksburg, MS: U.S. Army Engineer Research and Development Center.

Rushing, T. W., N. Torres, and Q. Mason. 2008. *AM2 10 CBR subgrade sensitivity test for the rapid parking ramp expansion program*. ERDC/GSL TR-08-13. Vicksburg, MS: U.S. Army Engineer Research and Development Center.

Rushing, T. W., and Q. S. Mason. 2008. *AM2 15 CBR subgrade sensitivity test for the rapid parking ramp expansion program*. ERDC/GSL TR-08-25. Vicksburg, MS: U.S. Army Engineer Research and Development Center.

U.S. Army Engineer Research and Development Center. 1995. *Standard test method for determining the California Bearing Ratio of soils*. CRD-C 654-95. Vicksburg, MS.

Appendix: Strain Gauge Data

Maximum MicroStrain Values Measured on F-15E Test Item										
Gauge #	ID	Pass Interval								
		1-10	11-16	17-32	33-48	49-80	81-112	113-126	127-128	129-136
62F1	Compression	-8698	-9983	-5426	-6848	*	*	*	*	*
	Tension	538	-2882	766	3826	*	*	*	*	*
62F2	Compression	-8064	-8382	-12745	-7046	*	*	*	*	*
	Tension	742	-1887	752	935	*	*	*	*	*
63F1	Compression	-3454	-3834	-3122	-3235	-1174	-49	-543	-143	-657
	Tension	1698	2390	1615	2604	2831	3283	2833	2048	2132
63F2	Compression	-1522	-1888	-3232	-2914	-4181	-383	-248	-197	-420
	Tension	2966	2836	1811	1953	1862	1710	1778	2395	2051
69F1	Compression	-4178	-3251	-3988	-5173	*	*	*	*	*
	Tension	539	135	673	814	*	*	*	*	*
69F2	Compression	-6457	-5295	-5365	-5276	*	*	*	*	*
	Tension	698	-705	638	689	*	*	*	*	*
70F1	Compression	-2711	-2584	-2359	-2439	-2310	-362	-298	-7	-268
	Tension	416	-3	349	710	617	924	1011	834	1182
70F2	Compression	-2367	-2469	-3420	-4170	-6026	707	-421	-181	-403
	Tension	2192	3290	2575	2892	6352	6352	4439	2247	2267
78F1	Compression	-2849	-3010	-2603	-3125	*	*	*	*	*
	Tension	416	599	1159	1563	*	*	*	*	*
78F2	Compression	-1307	-1556	-1344	-1804	*	*	*	*	*
	Tension	399	402	552	521	*	*	*	*	*
78F3	Compression	-4112	-4493	-3208	-4197	*	*	*	*	*
	Tension	788	-372	1218	1177	*	*	*	*	*
79F1	Compression	-4291	-4529	-3749	-4052	-5870	-983	-306	81	-503
	Tension	1561	1569	1413	3178	2242	1751	2702	1648	1828
79F2	Compression	-2893	-3125	-2818	-3070	-7724	-1922	-399	-123	-416
	Tension	1159	1027	1328	2583	2414	1354	2199	2001	1440
79F3	Compression	-2319	-1987	-2341	-3062	-4929	-1101	-674	-726	-1027
	Tension	2302	2979	2057	2287	2752	3808	3622	1106	2408
84F1	Compression	-3443	-3850	-3786	-4126	-4110	-1469	*	*	*
	Tension	525	155	550	579	1078	*	*	*	*
84F2	Compression	-1173	-1387	-1202	-1637	-1388	-800	*	*	*
	Tension	423	375	539	501	661	537	*	*	*

*Denotes gauge failure.

Maximum MicroStrain Values Measured on F-15E Test Item										
Gauge #	ID	Pass Interval								
		1-10	11-16	17-32	33-48	49-80	81-112	113-126	127-128	129-136
84F3	Compression	-1738	-1971	-1742	-2076	-2801	-2427	*	*	-6766
	Tension	784	1074	1418	1112	1387	1273	*	*	*
85F1	Compression	-2756	-3610	-3904	-4342	-4422	-5370	-7114	-903	-313
	Tension	2593	2956	1911	3141	2361	3278	2894	2384	1952
85F2	Compression	-2013	-2364	-1895	-2343	-2312	-1234	-8651	-1824	-483
	Tension	904	1123	1261	2233	2177	2486	1402	304	787
85F3	Compression	-2087	-2059	-2426	-3270	-5225	-5841	-3339	-156	-549
	Tension	3162	2903	2204	2655	2651	1996	1966	1335	2237
92F1	Compression	-3935	-4267	-5833	-6349	-4782	-4622	-3649	-214	*
	Tension	231	-92	287	455	771	1109	1579	418	*
92F2	Compression	-4809	-4787	-4875	-5725	-4943	-2751	-12022	-3414	*
	Tension	450	-238	239	302	327	536	281	-2556	*
93F1	Compression	*	*	*	*	*	*	*	*	*
	Tension	*	*	*	*	*	*	*	*	*
93F2	Compression	-2056	-1790	-2120	-2752	-2575	-593	-7593	-1564	-3794
	Tension	601	574	478	512	709	430	941	444	1348
98F1	Compression	-5979	-5901	-4427	-4728	-5256	-4722	-4847	-145	*
	Tension	1379	-322	1358	1369	1687	2132	1653	413	*
98F2	Compression	-5587	-6440	-5375	-5502	-5448	-4263	-10157	-3868	*
	Tension	810	-497	803	964	1457	1822	1754	-3050	*
99F1	Compression	-5830	-5781	-4380	-4865	-5022	-4792	-3664	33	-4774
	Tension	592	901	981	1865	1171	1518	2015	2287	2290
99F2	Compression	-4242	-4505	-5315	-7471	-5837	-4515	-6868	-920	-5523
	Tension	3620	4131	3770	4413	4695	5278	3623	2527	3174

*Denotes gauge failure.

Maximum MicroStrain Values Measured on C-17 Test Item				
Gauge #	ID	Pass Interval		
		1-12	13-28	29-56
60F1	Compression	-2986	-4225	-11687
	Tension	2286	3268	3314
60F2	Compression	-7753	-7731	-5490
	Tension	410	-1072	1708
61F1	Compression	-891	-734	-4407
	Tension	2911	2656	2011
61F2	Compression	-5691	-5642	-5140
	Tension	170	120	1028
66F1	Compression	-2291	-3383	-4880
	Tension	1186	1377	2246
66F2	Compression	-4640	-6870	-6428
	Tension	245	-129	-621
67F1	Compression	-2006	-4480	-5219
	Tension	3093	1538	404
67F2	Compression	-4550	-5473	-5219
	Tension	364	2	404
75F1	Compression	-2902	-3263	-8571
	Tension	1931	1545	2548
75F2	Compression	-1955	-1937	-4190
	Tension	453	285	392
75F3	Compression	-5519	-6656	-6737
	Tension	365	414	739
76F1	Compression	-1330	-2063	-6959
	Tension	1125	1393	1443
76F2	Compression	-2230	-2977	-2488
	Tension	-51	-29	153
76F3	Compression	*	*	*
	Tension	*	*	*
82F1	Compression	-5004	-20927	-17139
	Tension	1629	507	-7146
82F2	Compression	*	*	*
	Tension	*	*	*
82F3	Compression	-9538	-9251	*
	Tension	3061	*	*
83F1	Compression	-2396	-6390	-5915
	Tension	1196	867	2257
83F2	Compression	-2560	-2772	-1948
	Tension	315	238	614

*Denotes gauge failure.

Maximum MicroStrain Values Measured on C-17 Test Item				
Gauge #	ID	Pass Interval		
		1-12	13-28	29-56
83F3	Compression	-6546	-6630	-5530
	Tension	1033	66	2906
89F1	Compression	-10841	-10871	-864
	Tension	2037	632	3282
89F2	Compression	-5909	-16375	-7551
	Tension	1253	888	-4572
90F1	Compression	*	*	*
	Tension	1529	*	*
90F2	Compression	-4633	*	*
	Tension	771	*	*
96F1	Compression	-3527	-1344	-323
	Tension	1710	1789	3519
96F2	Compression	*	*	*
	Tension	833	18494	5719
97F1	Compression	-6398	*	*
	Tension	17412	*	*
97F2	Compression	*	*	*
	Tension	*	*	*

*Denotes gauge failure.

REPORT DOCUMENTATION PAGE

Form Approved
OMB No. 0704-0188

1. REPORT DATE *(DD-MM-YYYY)*	2. REPORT TYPE	3. DATES COVERED *(From - To)*
September 2014	Final	

4. TITLE AND SUBTITLE

AM2 3-4 Alternate Lay Pattern Evaluation

5a. CONTRACT NUMBER

5b. GRANT NUMBER

5c. PROGRAM ELEMENT NUMBER

6. AUTHOR(S)

Timothy W. Rushing, Lyan Garcia, Jeb S. Tingle, Paul G. Allison, and Craig A. Rutland

5d. PROJECT NUMBER

5e. TASK NUMBER

5f. WORK UNIT NUMBER

7. PERFORMING ORGANIZATION NAME(S) AND ADDRESS(ES)

Geotechnical and Structures Laboratory
US Army Engineer Research and Development Center
3909 Halls Ferry Road
Vicksburg, MS 39180-6199

8. PERFORMING ORGANIZATION REPORT NUMBER

ERDC/GSL TR-14-38

9. SPONSORING / MONITORING AGENCY NAME(S) AND ADDRESS(ES)

Air Force Civil Engineering Center
139 Barnes Drive, Suite 1
Tyndall AFB, FL 32403

10. SPONSOR/MONITOR'S ACRONYM(S)

AFCEC

11. SPONSOR/MONITOR'S REPORT NUMBER(S)

12. DISTRIBUTION / AVAILABILITY STATEMENT

Approved for public release; distribution is unlimited.

13. SUPPLEMENTARY NOTES

14. ABSTRACT

AM2 airfield matting has a long history of successful performance as an expeditionary airfield surfacing system. Logistical considerations for shipment of AM2 by the U.S. Marine Corps require equal numbers of 6-ft and 12-ft-long AM2 panels to be delivered to all project sites, resulting in far more 6-ft panels than are necessary to create a standard brickwork pattern. Therefore, the 3-4 alternate lay pattern was designed to allow Marines to use any mats on hand to fill in designated portions of the matted areas. Using the 3-4 pattern, as many as six continuous longitudinal joints are allowed, compared to only one with a brickwork pattern. A test section was constructed using the 3-4 pattern and trafficked by simulated F-15E and C-17 traffic. The test results showed a reduction in allowable passes of 92 to 96 % when compared to the brickwork pattern for an installation directly over a subgrade with a California Bearing Ratio of 6. Based on these results, the 3-4 pattern is not recommended for runways or high-speed taxiways, nor for soft soil installations.

15. SUBJECT TERMS

AM2
Landing Mat
Aluminum Mat
Airfield Mat
Airfield Damage Repair
Expeditionary Airfield Mat

16. SECURITY CLASSIFICATION OF:			17. LIMITATION OF ABSTRACT	18. NUMBER OF PAGES	19a. NAME OF RESPONSIBLE PERSON
a. REPORT	b. ABSTRACT	c. THIS PAGE			19b. TELEPHONE NUMBER *(include area code)*
Unclassified	Unclassified	Unclassified		77	